



UNIVERSIDAD DE INVESTIGACIÓN DE TECNOLOGÍA EXPERIMENTAL YACHAY

Escuela de Ciencias Químicas e Ingeniería

Characterization of Ecuadorian Ferruginous and Titaniferous Sands for Hydrogen Sulfide Capture

Trabajo de integración curricular presentado como requisito
para la obtención del título de Química

Autor:

Dayanna Carolina Vera Cedeño

Tutor:

Dr. Alex Uriel Palma Cando

apalma@yachaytech.edu.ec

Co-Tutor:

Dr. Marvin José Ricaurte Fernández

mricaurte@yachaytech.edu.ec

Urcuquí, Abril 2020

SECRETARÍA GENERAL
(Vicerrectorado Académico/Cancillería)
ESCUELA DE CIENCIAS QUÍMICAS E INGENIERÍA
CARRERA DE QUÍMICA
ACTA DE DEFENSA No. UITEY-CHE-2020-00022-AD

A los 14 días del mes de abril de 2020, a las 17:00 horas, de manera virtual mediante videoconferencia, y ante el Tribunal Calificador, integrado por los docentes:

Presidente Tribunal de Defensa	Dr. AVILA SOSA, EDWARD EBNER , Ph.D.
Miembro No Tutor	Dr. TORO ALAVA, JORGE EDUARDO , Ph.D.
Tutor	Dr. PALMA CANDO, ALEX URIEL , Ph.D.

El(la) señor(ita) estudiante **VERA CEDEÑO, DAYANNA CAROLINA**, con cédula de identidad No. **2300438401**, de la **ESCUELA DE CIENCIAS QUÍMICAS E INGENIERÍA**, de la Carrera de **QUÍMICA**, aprobada por el Consejo de Educación Superior (CES), mediante Resolución **RPC-SO-39-No.456-2014**, realiza a través de videoconferencia, la sustentación de su trabajo de titulación denominado: **Characterization of Ecuadorian Ferruginous and Titaniferous Sands for Hydrogen Sulfide Capture**, previa a la obtención del título de **QUÍMICO/A**.

El citado trabajo de titulación, fue debidamente aprobado por el(los) docente(s):

Tutor	Dr. PALMA CANDO, ALEX URIEL , Ph.D.
Co - Tutor	Dr. RICAURTE FERNÁNDEZ, MARVIN JOSÉ , Ph.D.

Y recibió las observaciones de los otros miembros del Tribunal Calificador, las mismas que han sido incorporadas por el(la) estudiante.

Previamente cumplidos los requisitos legales y reglamentarios, el trabajo de titulación fue sustentado por el(la) estudiante y examinado por los miembros del Tribunal Calificador. Escuchada la sustentación del trabajo de titulación a través de videoconferencia, que integró la exposición de el(la) estudiante sobre el contenido de la misma y las preguntas formuladas por los miembros del Tribunal, se califica la sustentación del trabajo de titulación con las siguientes calificaciones:

Tipo	Docente	Calificación
Miembro Tribunal De Defensa	Dr. TORO ALAVA, JORGE EDUARDO , Ph.D.	8,8
Presidente Tribunal De Defensa	Dr. AVILA SOSA, EDWARD EBNER , Ph.D.	9,4
Tutor	Dr. PALMA CANDO, ALEX URIEL , Ph.D.	9,0

Lo que da un promedio de: **9.1 (Nueve punto Uno)**, sobre 10 (diez), equivalente a: **APROBADO**

Para constancia de lo actuado, firman los miembros del Tribunal Calificador, el/la estudiante y el/la secretario ad-hoc.

Certifico que en cumplimiento del Decreto Ejecutivo 1017 de 16 de marzo de 2020, la defensa de trabajo de titulación (o examen de grado modalidad teórico práctica) se realizó vía virtual, por lo que las firmas de los miembros del Tribunal de Defensa de Grado, constan en forma digital.

VERA CEDEÑO, DAYANNA CAROLINA

Estudiante

EDWARD EBNER
 AVILA SOSA

Firmado digitalmente por
 EDWARD EBNER AVILA SOSA
 Fecha: 2020.04.14 19:16:31
 -05'00'

Dr. AVILA SOSA, EDWARD EBNER , Ph.D.

Presidente Tribunal de Defensa



Firmado electrónicamente por:

ALEX URIEL
PALMA CANDO

Dr. PALMA CANDO, ALEX URIEL , Ph.D.

Tutor



Dr. TORO ALAVA, JORGE EDUARDO , Ph.D.

Miembro No Tutor



Firmado electrónicamente por:

ANA MARIA
ESCOBAR
LANDAZURI

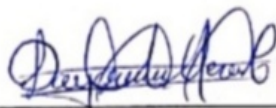
ESCOBAR LANDAZURI, ANA MARIA

Secretario Ad-hoc

Autoría

Yo, **DAYANNA CAROLINA VERA CEDEÑO**, con cédula de identidad **2300438401**, declaro que las ideas, juicios, valoraciones, interpretaciones, consultas bibliográficas, definiciones y conceptualizaciones expuestas en el presente trabajo; así como, los procedimientos y herramientas utilizadas en la investigación, son de absoluta responsabilidad de el/la autor(a) del trabajo de integración curricular. Así mismo, me acojo a los Reglamentos internos de la Universidad de Investigación de Tecnología Experimental Yachay.

Urcuquí, Julio 2020.



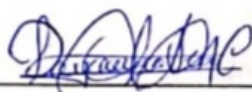
Dayanna Carolina Vera Cedeño

CI: 2300438401

Autorización de publicación

Yo, **DAYANNA CAROLINA VERA CEDEÑO**, con cédula de identidad **2300438401**, cedo a la Universidad de Tecnología Experimental Yachay, los derechos de publicación de la presente obra, sin que deba haber un reconocimiento económico por este concepto. Declaro además que el texto del presente trabajo de titulación no podrá ser cedido a ninguna empresa editorial para su publicación u otros fines, sin contar previamente con la autorización escrita de la Universidad. Asimismo, autorizo a la Universidad que realice la digitalización y publicación de este trabajo de integración curricular en el repositorio virtual, de conformidad a lo dispuesto en el Art. 144 de la Ley Orgánica de Educación Superior.

Urcuquí, Julio 2020.



Dayanna Carolina Vera Cedeño

CI: 2300438401

DEDICATORY

To my parents Frey Vera, Jessenia Cedeño, Favián Vera, Diana Vélez for their infinite support, love, comprehension, and patient during my academic formation; for their effort to help me become the person who I am now.

To my sisters Tatiana, Melanie and Helen for helping me to achieve my goals and support me, in their own way, in all this time.

To all my friends from Casa 7 for being the best people I could find, they will always be in my heart.

Dayanna Vera Cedeño

ACKNOWLEDGMENTS

Getting to where I am, has not been easy, I have received support from different people who have been with me in the good and bad times. First of all, I want to thank God for all of the blessings that I have: my parents, my sisters, my family, my friends, and my professors. Above all, thanks for giving me the strength to not give up and keep fighting until this part of my life is successfully completed.

I would like to thank INEDITA program for funding the Project number PIC-18-INE-YACHAY-001 in which I developed my job.

My sincere thanks to the people of Instituto Nacional de Patrimonio Cultural (INPC) for their contribution to the characterization process. Thanks to Dr. Martha Romero for her attentive reception at the laboratory facilities, and her instruction at work. Thanks to Chem. Carlos Vásquez for helping with Atomic Absorption Spectrophotometry guide and for helping me to rule out of all the problems that occurred. Thanks to Chem. Michelle Mármol for supporting with the EDS and XRD analysis. Thanks to Chem. Johanna Ramírez for her assistance with XRD and DLS analysis.

I also thank the Grupo de Investigación Aplicada en Materiales y Procesos (GIAMP), of Yachay Tech for make possible the development of this degree project.

Thanks to my advisor Dr. Alex Palma and co-advisor Dr. Marvin Ricaurte for their knowledge imparted throughout the development of this work, for their suggestions and support at each step.

I am very grateful to professors Dr. Edward Ávila, Dr. Jorge Toro, MSc. Lola de Lima, Dr. Manuel Caetano, and Dr. José M. Fernández for their assistance in the field and to improve the analysis of these results.

Thanks to all the people who be with me giving me their support and company.

Dayanna Vera Cedeño

ABSTRACT

Natural gas and oil extraction carried out by the hydrocarbon industry release acid gases; among them: hydrogen sulfide (H_2S), methane (CH_4) and carbon dioxide (CO_2). H_2S is a toxic, corrosive and flammable gas. At high concentrations, this gas can cause serious health problems and even death. For this reason, various methods for trapping H_2S have been designed including adsorption reaction on solid beds. One of the most used methods for H_2S removal is the use of SulfaTreat®, an environmentally friendly synthetic sand composed of iron oxide. Ecuador is a country rich in mineralogical resources. Black sands, composed by ferruginous and titaniferous minerals, show high content of iron and titanium oxides. In this work, thirteen sand samples were taken from different areas of Ecuador which, were dried, labeled, and stored for further physical and chemical analysis and characterization. The characterization of these sands was carried out through several methods: Dynamic Light Scattering (DLS), Atomic Absorption Spectrophotometry (AAS), Energy Dispersive Spectroscopy (EDS), and X-Ray Diffraction (XRD).

XRD analysis revealed most sand samples present silicon oxides as: Quartz, Feldspars, Pyroxenes, and Amphiboles mineral phases. DLS analysis indicated samples SXQ-102 and SYA-104 have a bigger surface area, that revealed the high adsorption capacity of these sands and its ability as good candidates for reactivity with H_2S for natural gas sweetening purposes. AAS analysis revealed sand samples SXQ-102 and SYA-104 have an elevated percentage of Iron: $17.9 \pm 0.7\%$ and $13.2 \pm 0.7\%$, respectively. EDS semi-quantitative analysis evidenced that sand samples with the highest percentage of iron and titanium oxides in their composition are SXQ-102 and SYA-104, with 11.84 % Fe and 1.42 % Ti, and 6.91 % Fe and 1.25 % Ti, respectively.

Samples with an elevated percentage of iron were magnetically enriched, characterized and reacted with hydrogen sulfide. Reacted sands were characterized by pH test, EDS and XRD techniques clearly pointing out for the absorption of sulfur in the samples. After EDS elemental analysis sulfur (S) and chlorine (Cl) appeared; while, XRD analysis indicated the presence of iron and titanium sulfides, which confirm the reactivity of these sands with the H_2S (g).

Keywords: *Black sands, hydrogen sulfide, solid beds, iron oxide, titanium oxide.*

RESUMEN

La extracción de petróleo y gas natural realizada por la industria de hidrocarburos libera gases ácidos; entre ellos: sulfuro de hidrógeno (H_2S), metano (CH_4) y dióxido de carbono (CO_2). El H_2S es un gas tóxico, corrosivo e inflamable. A altas concentraciones, este gas puede causar serios problemas de salud, e incluso la muerte. Por esta razón, se han diseñado varios métodos para atrapar H_2S , entre ellos, la reacción de adsorción en lechos sólidos. Uno de los métodos más utilizados para la eliminación de H_2S es el uso de SulfaTreat®, una arena sintética ecológica compuesta de óxido de hierro. Ecuador es un país rico en recursos mineralógicos. Las arenas negras, compuestas por minerales ferruginosos y titaníferos, muestran un alto contenido de óxidos de hierro y titanio. En este trabajo, se tomaron trece muestras de arena de diferentes áreas de Ecuador las cuales se secaron, etiquetaron y almacenaron para su posterior análisis y caracterización física y química. La caracterización de estas arenas se llevó a cabo mediante varios métodos: dispersión de luz dinámica (DLS), espectrofotometría de absorción atómica (AAS), espectroscopía de dispersión de energía (EDS) y difracción de rayos-X (XRD).

El análisis XRD reveló que la mayoría de las muestras de arena presentan óxidos de silicio como: fases minerales de cuarzo, feldespatos, piroxenos y anfíboles. El análisis de DLS indicó que las muestras SXQ-102 y SYA-104 tienen un área superficial más grande, lo que reveló la alta capacidad de adsorción de estas arenas y su capacidad como buenos candidatos para la reactividad con H_2S para fines de endulzamiento de gas natural. El análisis AAS reveló que las muestras de arena SXQ-102 y SYA-104 tienen un elevado porcentaje de hierro: $17.9 \pm 0.7\%$ y $13.2 \pm 0.7\%$, respectivamente. El análisis semi-cuantitativo de EDS evidenció que las muestras de arena con el mayor porcentaje de óxidos de hierro y titanio en su composición son SXQ-102 y SYA-104, con 11.84 % Fe y 1.42 % Ti, y 6.91 % Fe y 1.25 % Ti, respectivamente.

Las muestras con elevados porcentajes de hierro fueron enriquecidas magnéticamente, caracterizadas y reaccionadas con sulfuro de hidrógeno. Las arenas reaccionadas se caracterizaron por pruebas de pH, y las técnicas EDS y DRX mostrando claramente la absorción de azufre en las muestras. Después del análisis elemental EDS aparecieron azufre

(S) y cloro (Cl), mientras que, el análisis DRX indicó la presencia de sulfuros de hierro y titanio, lo que confirma la reactividad de estas arenas con el H_2S (g).

Palabras clave: *Arenas negras, sulfuro de hidrógeno, lechos sólidos, óxido de hierro, óxido de titanio.*

INDEX

<i>Autoría</i>	<i>iii</i>
<i>Autorización de publicación</i>	<i>iv</i>
<i>DEDICATORY</i>	<i>v</i>
<i>ACKNOWLEDGMENTS</i>	<i>vi</i>
<i>ABSTRACT</i>	<i>vii</i>
<i>RESUMEN</i>	<i>viii</i>
<i>List of Figures</i>	<i>xiii</i>
<i>List of Tables</i>	<i>xv</i>
<i>Abbreviations</i>	<i>xvi</i>
CHAPTER I: INTRODUCTION	1
CHAPTER II: LITERATURE REVIEW	2
2.1. Petroleum in Ecuador	2
2.2. Natural gas	3
2.3. Hydrogen sulfide	4
2.4. Sweetening of natural gas	5
2.4.1. Solid beds	5
2.5. SulfaTreat®-410 HP	5
2.6. Ecuadorian sands	6
CHAPTER III: PROBLEM STATEMENT	8
CHAPTER VI: OBJECTIVES	9
4.1. General Objective	9
4.2. Specific Objectives	9
CHAPTER V: METHODOLOGY	10
5.1. Ferruginous and titaniferous sands sampling	10
5.1.1. Sampling	10
5.1.2. Labeling	10
5.1.3. Drying and Storing	11
5.2. Characterization of natural sands	11
5.2.1. Dynamic Light Scattering	11
5.2.2. Atomic Absorption Spectrophotometry	12
5.2.2.1. Digestion process	13

5.2.2.2.	Preparation of standard solution	14
5.2.3.	Energy Dispersive Spectroscopy	14
5.2.4.	X-Ray Diffraction	15
5.3.	Reactivity	15
5.3.1.	Magnetic enrichment of natural sands	15
5.3.2.	Characterization of enriched black sands	16
5.3.3.	Reactivity of enriched black sands	17
5.3.4.	Characterization of reacted sands	17
5.3.4.1.	pH Tests	18
CHAPTER VI: RESULTS AND DISCUSSION		19
6.1.	Sands Sampling	19
6.1.1.	Sampling	19
6.1.2.	Labeling	20
6.1.3.	Drying and Storing	22
6.2.	Characterization of natural sands	23
6.2.1.	Dynamic Light Scattering	23
6.2.2.	Atomic Absorption Spectrophotometry	24
6.2.3.	Energy Dispersive Spectroscopy	26
6.2.4.	X-Ray Diffraction	27
6.3.	Reactivity	32
6.3.1.	Enrichment of natural sands	32
6.3.2.	Characterization of enriched black sands	33
6.3.2.1.	Dynamic Light Scattering for enriched sands	33
6.3.2.2.	Atomic Absorption Spectrophotometry for enriched sands	34
6.3.2.3.	Energy Dispersive Spectroscopy for enriched sands	34
6.3.2.4.	X-Ray Diffraction for enriched sands	35
6.3.3.	Reactivity of enriched black sands	37
6.3.4.	Characterization of reacted black sands	39
6.3.4.1.	pH Test of reacted sands	39
6.3.4.2.	Energy Dispersive Spectroscopy for reacted sands	39
6.3.4.3.	X-Ray Diffraction for reacted sands	40
CHAPTER VII: CONCLUSIONS AND RECOMMENDATIONS		43

7.1. Conclusions	43
7.2. Recommendations	44
BIBLIOGRAPHY	45
ANNEXES	49
Annex A	49
Sweetening of natural gas	49
<i>Acid gases absorption</i>	49
<i>Direct conversion</i>	50
<i>Chemical Captors</i>	51
<i>Semipermeable membranes</i>	51
<i>Extractive distillation</i>	52
<i>Solid beds</i>	52
Annex B	54
Annex C	54
Annex D	55

List of Figures

Figure 1: Principal Ecuadorian export products percentage.....	2
Figure 2: Drilling of a reservoir rock for petroleum extraction ⁴	3
Figure 3: Natural gas composition ⁵	3
Figure 4: SulfaTreat®-410HP ¹³	5
Figure 5: Schematic representation of a SulfaTreat® particle: the pellet is composed by fine iron oxide grains	6
Figure 6: Dug for sampling. Geologist hammer height is ≈ 80 cm.....	10
Figure 7: Codification label for sample SXQ-101.....	11
Figure 8: Process to follow to dry sands.	11
Figure 9: Atomic Absorption Spectrophotometer-7000 ³⁰	12
Figure 10: Acid digestion process.	14
Figure 11: Sample tablet for EDS analysis.	15
Figure 12: Magnetic separation of natural sands.	16
Figure 13: Reactivity set up.	17
Figure 14: Macherey-Nagel 921 10 color-fixed pH indicator paper scale. (Source: Macherey-Nagel, 2020)	18
Figure 15: Sampling areas of the first field trip. (Map retrieved from Google maps).....	19
Figure 16: Sampling areas of the second field work. (Source: Google maps).....	20
Figure 17: Comparison between wet (left) and dry (right) sand sample SET-203. (Source: Jorge Toro, PhD)	22
Figure 18: Water presence in natural sands.....	23
Figure 19: Iron percentage in natural sand samples determined by applying the AAS.....	26
Figure 20: X-ray diffraction pattern of SXQ-102 sample. Included the percentage table of mineral phases present in the sample: Quartz (Qz), Feldspar (Fs), Pyroxene (Px), Amphibole (Amph), and Oxides (Ox).....	28
Figure 21: X-ray diffraction pattern of SYA-104. Included the percentage table of mineral phases present in the sample: Quartz (Qz), Feldspars (Fs), Pyroxenes (Px), Amphiboles (Amph), Oxides (Ox), and Carbonates(Cb)	29
Figure 22: Enriched black sands.....	33
Figure 23: Iron percentage in enriched sands by AAS.....	34
Figure 24: X-ray diffraction pattern for enriched black sand sample SXQ-102. The inset includes the percentage of mineral phases in the sample.	36
Figure 25: X-ray diffraction pattern for enriched black sand sample SYA-104. The inset includes the percentage of mineral phases in the sample.	37
Figure 26: Reactivity setup	38
Figure 27: Black sand sample SXQ-102 before(left) and after (right) reacting with Hydrogen Sulfide.	38
Figure 28: pH test results. Enriched sands: pH 7; Reacted sands: pH 3 (SXQ-102), and pH 2 (SYA-104)....	39

Figure 29: X-ray diffraction pattern for reacted sand sample SXQ-102. The inset includes the percentage of mineral phases in the sample.....	41
Figure 30: X-ray diffraction pattern for reacted sand sample SYA-104. The inset includes the percentage of mineral phases in the sample.....	42
Figure 31: Triazine captor and hydrogen sulfide reaction. (Source: Pirkko, 2019, https://slideplayer.com/slide/15321919/).....	51
Figure 32: Tiling representation of the structure of the zeolite L (LTL). Blue tiles are channels in the structure running along direction of the crystallographic c axis ⁴⁰	53
Figure 33: X-ray diffraction pattern for natural sand sample SXQ-101. The inset includes the percentage of mineral phases in the sample.....	55
Figure 34: X-ray diffraction pattern for natural sand sample SXQ-102. The inset includes the percentage of mineral phases in the sample.....	56
Figure 35: X-ray diffraction pattern for natural sand sample SYA-103. The inset includes the percentage of mineral phases in the sample.....	57
Figure 36: X-ray diffraction pattern for natural sand sample SYA-104. The inset includes the percentage of mineral phases in the sample.....	58
Figure 37: X-ray diffraction pattern for natural sand sample SYO-105. The inset includes the percentage of mineral phases in the sample.....	59
Figure 38: X-ray diffraction pattern for natural sand sample SYM-106. The inset includes the percentage of mineral phases in the sample.....	60
Figure 39: X-ray diffraction pattern for natural sand sample SEV-201. The inset includes the percentage of mineral phases in the sample.....	61
Figure 40: X-ray diffraction pattern for natural sand sample SET-202. The inset includes the percentage of mineral phases in the sample.....	62
Figure 41: X-ray diffraction pattern for natural sand sample SET-203. The inset includes the percentage of mineral phases in the sample.....	63
Figure 42: X-ray diffraction pattern for natural sand sample SMP-204. The inset includes the percentage of mineral phases in the sample.....	64
Figure 43: X-ray diffraction pattern for natural sand sample SEM-205. The inset includes the percentage of mineral phases in the sample.....	65
Figure 44: X-ray diffraction pattern for natural sand sample SEM-206. The inset includes the percentage of mineral phases in the sample.....	66
Figure 45: X-ray diffraction pattern for natural sand sample SEG-207. The inset includes the percentage of mineral phases in the sample.....	67

List of Tables

Table 1: Side effects of H ₂ S according to time and concentration of exposition.	4
Table 2: Natural sands information used to generate sample codification.	21
Table 3: Particle size information of natural sands.....	23
Table 4: Iron concentration of standard solutions and absorbance	24
Table 5: Iron concentration of sample solutions and absorbance.....	24
Table 6: Chemical semi-quantitative composition of sand sample, expressed in oxides, by SEM-EDS analysis.	26
Table 7: Mineral phases of natural sands.	30
Table 8: Particle size data about enriched sands.....	33
Table 9: Chemical composition of enriched sands by SEM-EDS analysis, expressed as oxides.....	35
Table 10: Mineral phases present in enriched sands by XRD analysis	35
Table 11: Chemical composition of reacted sands by SEM-EDS analysis.....	40
Table 12: Mineral phases of reacted sands.....	40

Abbreviations

AAS Atomic Absorption Spectrophotometry

COD Crystallography Open Database

DLS Dynamic Light Scattering

EDS Energy Dispersive Spectroscopy

INPC Instituto Nacional de Patrimonio Cultural

NGP Natural Gas of Petroleum

SEG Sand sample from Esmeraldas – Punta Galera beach

SEM Sand sample from Esmeraldas – Mompiche beach

SET Sand sample from Esmeraldas – Tonsupa beach

SEV Sand sample from Esmeraldas – Río Verde beach

SMP Sand sample from Manabí – Pedernales beach

SXQ Sand sample from Cotopaxi – Quilotoa volcano

SYA Sand sample from Santa Elena – Anconcito beach

SYM Sand sample from Santa Elena – Montañita beach

SYO Sand sample from Santa Elena – Olón beach

XRD X-ray Diffraction

CHAPTER I: INTRODUCTION

Petroleum is a fossil fuel used as a raw material to produce almost all the industrial products humankind enjoy in current days. In Ecuador, the extraction and exportation of petroleum is the main source of income in the economy. However, natural gas and oil extraction releases acid gases; among them, hydrogen sulfide (H_2S), methane (CH_4) and carbon dioxide (CO_2). Hydrogen sulfide is a toxic, corrosive and flammable gas, harmful to human health, and risky for facilities because its corrosivity. For these reasons, various methods for trapping hydrogen sulfide have been designed, including adsorption reaction on iron oxides. Ecuador is a country rich in mineralogical resources, with igneous and sedimentary rocks rich in iron and titanium minerals, among them magnetite and ilmenite in black sands. Accordingly, they have been of main mining interest for years.

This work aims to find out a method to capture hydrogen sulfide based on the use of ferruginous and titaniferous black sands collected in different areas of Ecuador. The provinces where the sampling process was carried out were Cotopaxi, Santa Elena, Esmeraldas, and Manabí. Characterization of these sands was carried out in the Chemistry Laboratory of the Instituto Nacional de Patrimonio Cultural (INPC), in Quito. The enrichment and reactivity of sands were performed in Yachay Tech laboratories.

Chapter II shows some concepts that support the development of this work, among them: the petroleum production in Ecuador; the release of natural gas and its composition; the acid gases, such as H_2S , its effects, and some methods for trapping it. Chapters III and IV announce, respectively, the problem statement, addressed with its corresponding justification, and the objectives to be achieved in this study.

Chapter V indicates a detailed procedure followed to carry out this work, as well as, the techniques used during the experimental part, which is organized in three stages: sands sampling, characterization and reactivity of sands with H_2S . Chapter VI expresses the results and discussions obtained from sampling, labeling, drying, characterization by using different analytical techniques, enrichment, and reactivity. Finally, Chapter VII exhibits the conclusions of this work, and some recommendations succeeded along with the study.

CHAPTER II: LITERATURE REVIEW

2.1. Petroleum in Ecuador

Petroleum is considered the main raw material used for the elaboration of most of the industrial products existing in these days. The production and consumption of oil have been increasing through the last years¹. In Ecuador, the extraction and exportation of petroleum have been considered as the main source of income in the economy². In addition to oil, Ecuador exports several primary products, including: shrimp, cocoa, tuna fish, canned fish, natural flowers, mining products, wood, among others (see Figure 1). According to Banco Central del Ecuador (2019), the exportation of petroleum and its derivatives represents 40.10% of the total exported products. In fact, it means \$ 6,715,289 from the \$ 16,747,018 which is the total exportation capital revenue³.

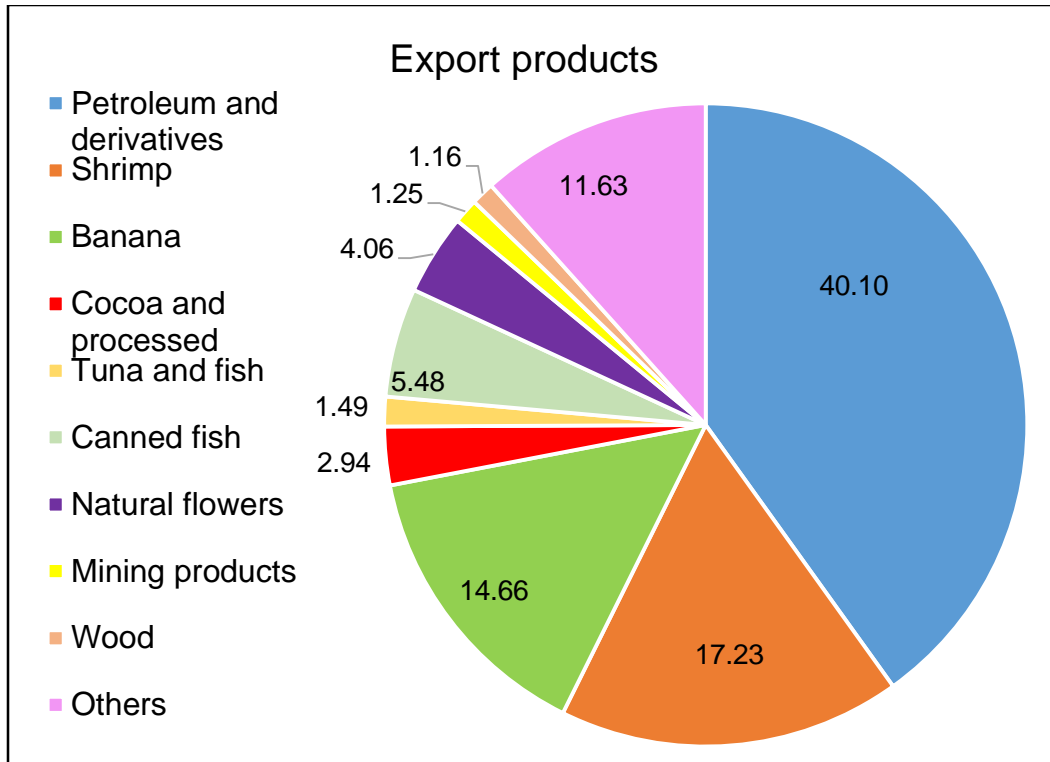


Figure 1: Principal Ecuadorian export products percentage³.

Being this fossil fuel widely used in daily life, hydrocarbon industries are also focused on its effect on the environment. The oil extraction process, consists of the drilling of the substratum, until arriving to and providing the reservoir rock, by using wells (see Figure 2). After drilling the well and installing a casing, to produce crude oil, a metallic tube goes down

the ground to perforate the casing at the height of interest, the reservoir. Then, the oil flows through the perforations to a smaller tube, and due to the underground pressure, it reaches the surface accompanied by formation water and, in most cases, natural gas⁴.

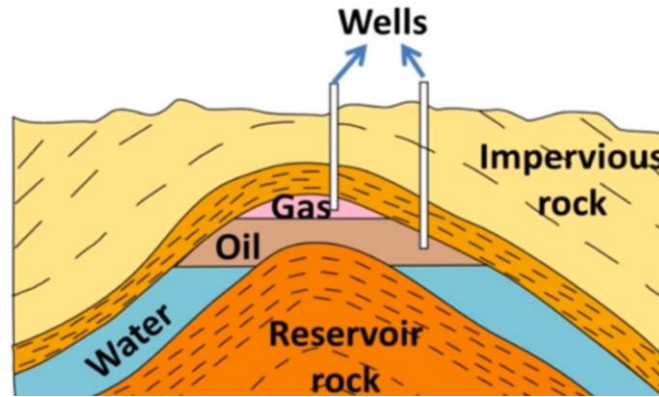


Figure 2: Drilling of a reservoir rock for petroleum extraction⁴.

2.2. Natural gas

Natural gas of petroleum (NGP) is a mixture of several gases, among them hydrocarbon, non-hydrocarbons, and inert gases (see Figure 3). Hydrocarbon gases refer to paraffinic hydrocarbon (C_1 to C_{11}): methane (CH_4), ethane (C_2H_6), propane (C_3H_8), butane (C_4H_{10}), to undecane ($C_{11}H_{24}$)⁵. Among the Non-hydrocarbon gases, considered as impurities, are the acid gases hydrogen sulfide (H_2S) and carbon dioxide (CO_2), there are also other gases such as water vapor. Inert gases are Helium (He), Argon (Ar), Hydrogen (H_2), Oxygen (O_2), Nitrogen (N_2), and others⁶.

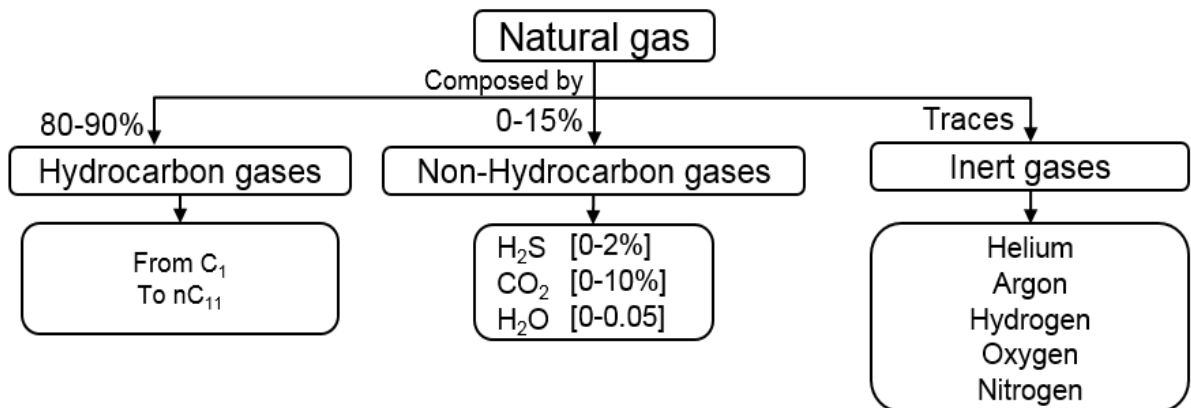


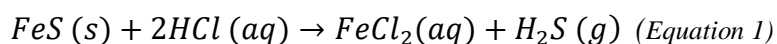
Figure 3: Natural gas composition⁵.

Natural gas can be directly obtained from gas wells, condensed wells, or from oil wells as an output product in the petroleum extraction process^{5,7}. This gas passes through a processing plant to be purified from acid gases, heavy hydrocarbons, and other impurities.

2.3. Hydrogen sulfide

Hydrogen sulfide (H₂S) is an invisible, toxic, flammable, and corrosive gas recognized by its characteristic rotten eggs odor. Its physical properties are: molecular mass (34 g/mol), melting point (-86 °C), boiling point (-60 °C), vapor pressure (1880 kPa), and solubility in water (3980 mg/L)⁸. It is also known as sewer gas, swamp gas, manure gas, and stink gas⁹.

H₂S is part of the impurities present in natural gas; however, it can be obtained in different ways. Hydrogen sulfide can be found in groundwater and inside the ground, present in crude oil, natural gas, volcanic gases, or hot springs. Also, it can be formed by the anaerobic bacterial reduction of sulfates and organic compounds that contain sulfur.¹⁰ Furthermore, hydrogen sulfide can be obtained by the exothermic reaction of iron sulfide (FeS) with hydrochloric acid (HCl) to form the acid gas and iron chloride as products (see Equation 1).



The exposition of H₂S in humans, is by inhalation, principally. The gas is absorbed through the lungs and then is metabolized in the organism by oxidation, methylation, and reactions with proteins that contain disulfides. The nervous and cardiac tissues are the most sensitive organs to this effect¹⁰. Depending on the time and concentration of exposure, this gas can cause severe harm to human health. Its effects range from irritability to breathing, nausea, dizziness, vomiting, headaches, loss of smell sense, to fainting and death (see Table 1)¹¹.

Table 1: Side effects of H₂S according to time and concentration of exposition.

Side effects of H ₂ S exposure		
Concentration [ppm]	Time of exposition	Effect
10	8 hours	Unpleasant smell.
70-169	> 1 hour	Slight symptoms such as dizziness, or nausea.
170-300	< 1 hour	Irritation to the respiratory system.
301-500	> 30 minutes	Risk to human health.

2.4. Sweetening of natural gas

The sweetening of natural gas consists of the purification process in which amounts of acid gases, such as hydrogen sulfide (H₂S) and carbon dioxide (CO₂), are controlled. It is important to remove the H₂S because it causes corrosion of facilities when it interacts with CO₂ and water vapor. Currently, there are several methods for trapping H₂S from natural gas (see Annex A). The selection of the best option to sweeten the natural gas will depend on the applicability of the method, the economy involved in the process, and the effectiveness. Among the techniques used to capture hydrogen sulfide are: chemical, physical, and physical-chemical absorption; direct conversion of hydrogen sulfide to sulfur; solid and liquid captors, semipermeable membrane; extractive distillation; and solid beds. The amount of acid that will be removed will depend on the sweetening method chosen¹¹.

2.4.1. Solid beds

Solid beds are products commonly used in gas industries. The acid gases removal is realized by an adsorption process which, depending on the material surface to use, it can be chemical or physical¹². This technique uses molecular sieves, iron sponge, zinc oxide, or SulfaTreat®, as solid beds. For solid beds based on iron and zinc oxides, the reaction is chemical and irreversible; while, for molecular sieves, the reaction is physical and reversible¹².

2.5. SulfaTreat®-410 HP



*Figure 4: SulfaTreat®-410 HP*¹³.

SulfaTreat®-410 HP (see Figure 4) is a commercial product used to capture hydrogen sulfide and mercaptans (RSH) from natural gas flow¹⁴. It consists of an artificial sand mainly composed of iron oxide and silica oxide. It is an environmentally friendly product, so its

management does not require much caution, even when reacted¹⁵. Its maintenance must be performed every 330 days¹¹.

SulfaTreat® works at temperatures between 18-25°C, and resists up to 100 ppm of hydrogen sulfide. This material is characterized by its simplicity, uniform shape, and economic price; however, the maintenance is a little bit expensive¹⁶.

SulfaTreat® has high selectivity with sulfides. When the impurities are removed from the natural gas, they are captured by the iron oxides in the bulk of the material (see Figure 5)¹⁷. SulfaTreat® is capable to adsorb acid gases until it is totally covered, so it must be replaced when the intake gas is equal to that of the outlet gas.

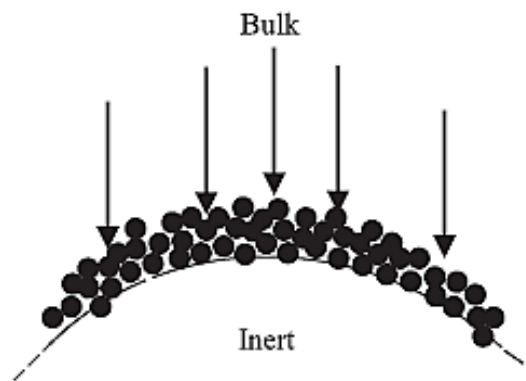


Figure 5: Schematic representation of a SulfaTreat® particle: the pellet is composed by fine iron oxide grains

(●) attached to the surface of an inert support¹⁷.

When H₂S reacts with SulfaTreat®, it forms pyrite (FeS₂) which is the most common sulfide mineral (see Equation 2). Pyrite is a stable compound that does not decompose easily, if not mixed with water (L), and it is not toxic, so it can be safely discarded¹⁸.



2.6. Ecuadorian sands

Ecuador is a country with a privileged mineral richness, located on the northwest of South America. Ecuador participates in the convergence between the South American and Nazca plates which join from 5.5 to 5.8 cm per year. This movement gives rise to The Andes Highlands continuously producing seismic movements and volcanism¹⁹.

Due to earth movements, volcanic eruptions and other phenomena, some rock fragments are ejected from the earth. On the earth's surface, factors like atmosphere, wind, rain, changes in pressure and temperature, alter and erode the rocks²⁰. When going through the erosion process, rocks are disintegrated, and their sediments are transported to the ocean by the action of rivers. The transportation process classifies the grains according to their size and toughness²¹. The size and shape of the final grain will depend on the distance traveled and how it was eroded. Grains that are transported by rivers, are deposited on the shoreline which then, are washed out by the waves to form beaches. The color of the sand is due to the material of its particles; that is, light colored sands belong to the presence of quartz, while the blackish sands will present iron minerals²².

In Ecuador, sands present high concentrations of iron and titanium oxides, with approximate values of 10-60% and 35%, respectively²³. Black sands of Ecuador have been of main mining interest during years due to their elevated concentration of iron and titanium minerals²⁴. Some construction industries take advantage of ferruginous and titaniferous sands for building purposes; such as cement production²².

CHAPTER III: PROBLEM STATEMENT

Oil extraction releases natural gas which is a mixture of several gases. One of them is hydrogen sulfide. When this acid gas reacts with carbon dioxide and water vapor, it causes corrosion in the equipment and facilities. In addition, there are severe problems that the release of this acid gas cause to human health. That is why it is important to capture the H₂S in a process known as sweetening of natural gas. Currently, several methods for trapping it are known, but one of the most applied in the hydrocarbon industry is the use of SulfaTreat®-410 HP. This material is a non-hazardous artificial sand mainly composed of iron oxide and different silicon oxides.

In this work, it is intended to replace the technology of SulfaTreat®-410 HP by using ferruginous and titaniferous sands collected in Ecuador. Black sands of Ecuadorian beaches are recognized by its composition rich in iron and titanium minerals. As previously mentioned, iron oxides are good adsorbents of H₂S; however, titanium oxides generate stable sulfides too, such as titanium sulfide (Ti₂S₃)²⁵. To carry out this work, sand samples from some areas of the country had been taken. Then, the collected sands passed through processes of characterization, enrichment, and reactivity with hydrogen sulfide. Finally, a comparison of sands before and after reacting will be made to prove the adsorption of sulfur in sands.

CHAPTER VI: OBJECTIVES

4.1. General Objective

To characterize several ferruginous and titaniferous Ecuadorian sands applied in the capture of hydrogen sulfide.

4.2. Specific Objectives

To collect thirteen black sand samples from different areas of Ecuador.

To characterize the sands samples size by using Dynamic Light Scattering.

To identify the sand samples composition through: Atomic Absorption Spectrophotometry (AAS), Energy Dispersive Spectroscopy (EDS), and X-Ray Diffraction (XRD).

To perform the magnetic enrichment of iron mineral from natural sands which present high contents of iron and titanium oxides.

To test enriched sands reactivity with hydrogen sulfide.

CHAPTER V: METHODOLOGY

5.1. Ferruginous and titaniferous sands sampling

5.1.1. Sampling

Thirteen sand samples were collected from different provinces of Ecuador; among them, Cotopaxi, Santa Elena, Esmeraldas, and Manabí. The sampling processes were carried out in two field works. Sand samples obtained in the central Andes ridge, in Cotopaxi province, were directly collected from the soil surface; while sand samples from the Ecuadorian Coastal zone were collected from the beach zone. To obtain a representative sample of the beach area, a 50 cm depth hole was dug to take the sample from all the edge part^{26,27} (see Figure 6). Approximately, 9 kg of each sample were stockpiled into plastic bottles for further treatments.



Figure 6: Dug for sampling. Geologist hammer height is ≈ 30 cm.

5.1.2. Labeling

Labeling of sand samples consisted of a code of three letters and three numbers for each of them. The first letter, S, is for Sand; the second one belongs to the province codification, and the third one indicates the place where the sample was picked up. In the case of the numbers, the first one shows the sampling campaign, and the next two numbers correspond to the sample collected in each trip. As an example, the codification assigned for the first sand sample taken in the foothills of the Quilotoa volcano is showed in Figure 7.

S	X	Q	-	1	0	1
---	---	---	---	---	---	---

Figure 7: Codification label for sample SXQ-101

5.1.3. Drying and Storing

To dry the sand, first, the initial weight of the sand was recorded. Then, the sample was introduced in an oven at 90 °C to remove water from the sand. After passing one hour, the sample was taken out from the oven to register its current weight. The process was repeated each hour until obtaining a constant weight in the sample (see Figure 8). Finally, the water loses percentage curve was plotted using the recorded data.

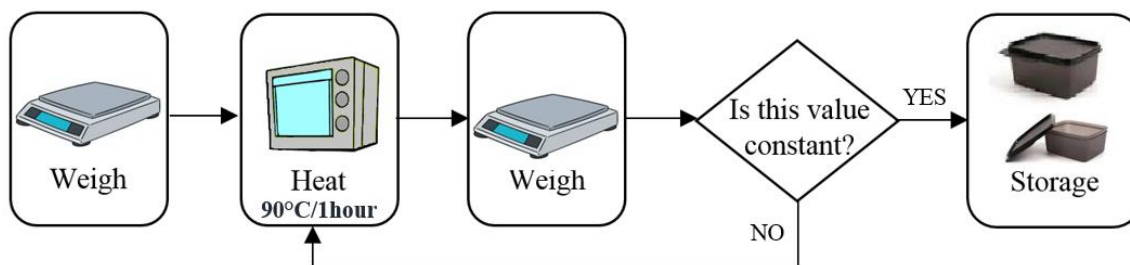


Figure 8: Process to follow to dry sands.

5.2. Characterization of natural sands

5.2.1. Dynamic Light Scattering

Dynamic light scattering (DLS) is a technique used to determine the size of a particle whose rank oscillates between 100 nm and 1000 µm. This technique consists in the pass of particles through a light beam, where the scattering angle of light is related to the particle size. Then, big particles disperse at low angles and small particles at high angles²⁸. The size of the particle indicates the adsorption capacity of it, the smaller the surface area of the particle, the greater its contact surface will be, so it will give way to greater adsorption²⁹.

The measurement of the particle size was realized by using a HORIBA LA-950V2 device. Particles with a grain size bigger than 1 mm were passed through a sieve N° 100 (size: 150 µm).

5.2.2. Atomic Absorption Spectrophotometry

The concentration of iron was measured by using the flame method of the atomic absorption spectrophotometry (AAS). This technique is based on Lambert-Beer's law which states that, at a certain wavelength, the absorbance of a sample depends on the concentration of the transmitted light³⁰. This method establishes that when an atom absorbs external energy, it is moved up from the ground state (or most stable state) to the excited state (or less stable state). When the atoms returns to the stable state, it emits energy in form of light at a characteristic wavelength for each element³¹. The concentration of the element in the sample will depend on the amount of energy absorbed in the flame³². This technique demands the preparation of both standard and sample solutions. To prepare the sample solutions, it was required to digest the sand samples with concentrated acids such as nitric acid (HNO₃), perchloric acid (HClO₄), hydrochloric acid (HCl), and hydrofluoric acid (HF) (see Figure 10). To turn on the AAS device, the pass of the gases air, acetylene (NU-1001), and nitrous oxide (NU-1070), was opened considering not to exceed the limit pressure for each one: 50, 15, 50-60 psi, respectively³³. Then, the solution of digestion was injected into the flame of the Atomic Absorption Spectrophotometer AAS-7000 (see Figure 9), at a wavelength of 294.4 nm, and a burner height of 7 mm. The lamp used for flame was BGC-D2 for iron. The standard solutions for iron were diluted to 40, 120, and 200 ppm, and were used to obtain the calibration curve in the program WizAArd. Finally, by using the software WizAArd, the concentration of iron for each sand sample was measured.



Figure 9: Atomic Absorption Spectrophotometer-7000³⁴.

5.2.2.1. Digestion process

The digestion of sand samples was carried out by following a protocol taken from the *Instituto Nacional de Patrimonio Cultural* (INPC)³⁴. First, it was important to clean the required equipment, and use gloves, glasses and safety mask during all the process. Then, 0.4000 ± 0.0001 g of sand were weighed into a Teflon glass previously labeled using the code for each sample. Inside a fume hood, to dissolve carbonates, 2.0 ± 0.1 mL concentrated nitric acid (HNO_3 69-70 %) were added and stirred gently to homogenize; then, 2.0 ± 0.1 mL concentrated (HClO_4 70-72 %) were added and homogenized. Operators must be covered with a watch glass and heat the solution on the hot plate settled at 135°C . Remove the Teflon glass from heat when the solution is almost dry, and let cool at room temperature.

To dissolve metals present in sands, it was added 5.0 ± 0.1 mL HNO_3 69-70 % and 7.0 ± 0.1 mL concentrated hydrochloric acid (HCl 38 %), homogenized, covered, and heated on the hot plate (see Figure 10). Once the solution was almost dried, it was retired from heat and cooled at room temperature. To dissolve silicates, it was used 10 mL of concentrated hydrofluoric acid (HF 48%), homogenized, and heated to almost dryness. Then, it was retired from heat and allowed to cool. The excess of HF was eliminated with the addition of 1mL HCl 38%, homogenized, and heated until it was dried. To dissolve the remaining salts, 5mL HCl 38% were added and heated at a lower temperature (85°C).

The resulting digest was filtered through a Macherey-Nagel 615 (125 mm) filter paper, and the filtered digested solution was rinsed and transferred to a 100 mL volumetric flask, and filled up until the mark with deionized water type 1. The dilution inside the volumetric flask was transferred to a 125 mL plastic bottle and labeled to be analyzed in the atomic absorption spectrophotometer equipment.

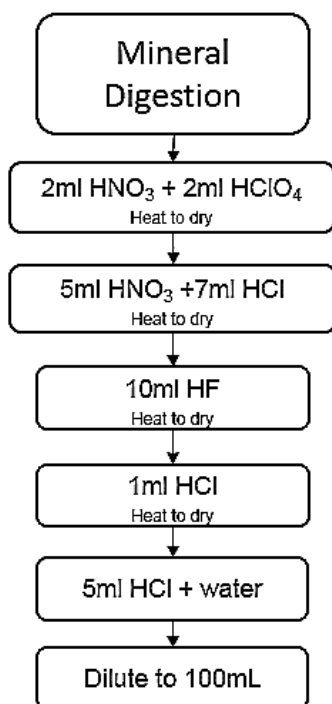


Figure 10: Acid digestion process.

5.2.2.2. Preparation of standard solution

The standard solutions for each element were prepared based on the SHIMADSU atomic absorption spectrophotometer guide book³². For iron standard solutions, the concentrations prepared were 0, 40, 120, and 200 ppm. Parting from a 1000 ppm solution, it was prepared 10 mL iron standard solution to each concentration.

5.2.3. Energy Dispersive Spectroscopy

To obtain an elemental semi-quantitative/qualitative analysis of the composition of the sand, it was used Energy Dispersive Spectroscopy (EDS). This technique is based on the detection of X-rays emitted by a sample after being excited by an electron beam to determine the elements present in the surface of that sample at a certain depth³⁵. The X-rays are captured in a spectrum that provides both semi-quantitative and semi-qualitative information about the amount of each element present in the sample³⁶. This technique required the elaboration of compact tablets of the sample before being analyzed (see Figure 11). To do this, 2.5 g - 3 g sand sample (sieved to 75 μm) were mixed and homogenized with 2 g - 2.5 g cellulose and compressed by using a pressing machine. Once the sample was compacted, it was carefully placed on the Jeol IT300 microscope holder to be analyzed by using a program called Aztec.

The settled parameters were height from the detector (12 mm-14 mm), and the voltage (20 kV – 30 kV).



Figure 11: Sample tablet for EDS analysis.

5.2.4. X-Ray Diffraction

To determine the mineral phases, present in sands, and its percentage mineralogical composition, samples were measured by the powder X-ray diffraction technique (XRD). Crystalline materials have atoms arranged in a periodic way, which, when are incised by X-rays, diffract light. Then, the wavelength of the X-ray will depend on the distance between the atoms. This technique consists of the diffraction of X-rays to produce a diffraction pattern which contains the information of the arrangement of atoms inside the material³⁷. To carry out this technique; first, sand samples size was reduced by using an agate mortar and passed through a sieve N°200 to obtain a homogenous size of $< 75 \mu\text{m}$. Then, the powder was fitted into the diffractometer holder which was introduced in the device. By using the X-Ray Diffractometer BRUKER D8-ADVANCE of INPC, the parameters settled to measure the sample were a copper anode ($\lambda=1.5406 \text{ \AA}$), scanning 2θ angle of 10° to 60.976° with a rotation of the sample of 15.000 (1/min), in steps of 0.015° ²⁸.

5.3. Reactivity

5.3.1. Magnetic enrichment of natural sands

To increase the content of iron oxides in the natural sands, it was realized the magnetic enrichment of metallic fragments by using a magnetic separator, such as a magnet. This kind of separator is commonly used for less than 0.5 cm in diameter grains because it allows to have a cleaner final product and avoid unnecessary sample loss³⁸.

The enrichment of sand samples SXQ-102 and SYA-104 was carried out through wet magnetic separation by employing a plastic covered magnet with a magnetic field 0.1 T³⁹. For sand sample SXQ-102, 230.0 g of sieved sand (D>100 μm) were weighed into a 500 mL beaker. Then, the sand sample was washed/soaked with 100 mL of distilled water, and from the outside of the beaker, the particles were attracted with a magnet (see Figure 12). Once the magnetic particles were attracted to the magnet, the water inside the beaker was drained into a smaller beaker, and the particles attracted to the magnet were removed into a petri dish. Then, the magnet was covered by a plastic film, and it was introduced inside the sand drained before completely remove the magnetic particles. This process was repeated until no magnetic particles were attracted to the magnet. For sand sample SYA-104, 250 g natural sand were weigh in a 500 mL beaker. Then, the wet magnetic separation was performed in the same way as the SXQ-102 sample. Finally, the enriched sand was dried and its weight was recorded to obtain its yield (See Equation 3).

$$\text{Enrichment Yield} = \frac{\text{enriched sand weigh}}{\text{natural sand weigh}} * 100 \quad (\text{Equation 3})$$

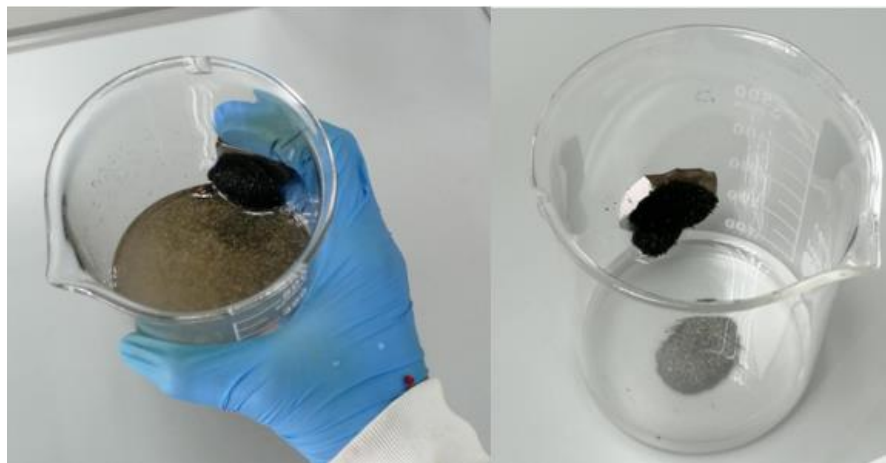


Figure 12: Magnetic enrichment of natural sands.

5.3.2. Characterization of enriched black sands

Physical and chemical characteristics of enriched black sands were determined by using Dynamic Light Scattering (DLS), Atomic Absorption Spectrophotometry (AAS), Energy Dispersive Spectroscopy (EDS), and X-Ray Diffraction (EDS) techniques. The process was carried out in the same way as natural sands characterization and using the same conditions.

5.3.3. Reactivity of enriched black sands

The reactivity of enriched sands was carried out by following Equation 1. To do that, 10.00 ± 0.01 g - 10.50 ± 0.01 g of sand sample were placed inside a 250 mL round bottom flask. Also, a test tube containing 1.00 ± 0.01 g - 1.10 ± 0.01 g FeS was introduced in the round bottom flask. The system was closed by using a septum plug (see Figure 13). Then, using a syringe, 3 mL HCl (38%) were added to the FeS. After a week, HCl (38%) was added to the test tube. A week later, the gas was purged into a NaOH 3.5M solution, and the sand was carefully weighed and stored. It is important to remember that the gas inside the flask is highly toxic, so this process must be carried inside a fume hood, and the use of protective glasses and mask is recommended.

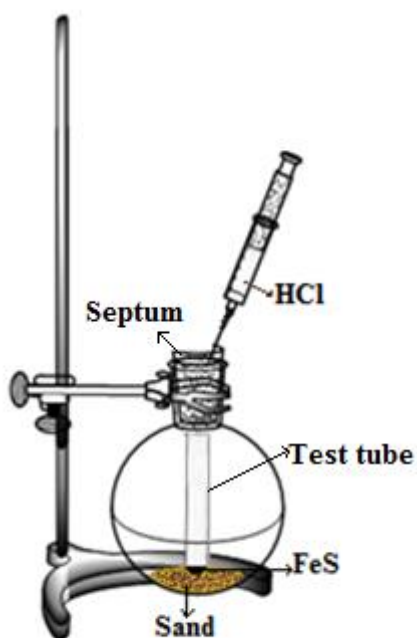


Figure 13: Reactivity set up.

5.3.4. Characterization of reacted sands

Reacted sands were characterized by pH test, energy dispersive spectroscopy, and X-ray diffraction techniques. The process to follow was the same as enriched sands, this time, it was necessary to take special care in the security measures, since the sand samples had reacted with acid. That is, it was demanded to wear a special mask for acid gases, safety goggles, and gloves.

5.3.4.1. pH Tests

To obtain the pH of reacted samples, it was taken 0.50 ± 0.1 g of sand into a petri dish. Then, 15 mL of Type-1 distilled water were added, and the sand was mixed through a magnetic stirring. Finally, by using a Macherey-Nagel 921 10 color-fixed pH-indicator paper (see Figure 14), its pH was measured. To compare the results, the pH of distilled water was tested as a blank solution.



Figure 14: Macherey-Nagel 921 10 color-fixed pH indicator paper scale⁴⁰.

CHAPTER VI: RESULTS AND DISCUSSION

6.1. Sands Sampling

6.1.1. Sampling

The first sampling field trip took place from July 16th to July 19th, 2018, with the collection of two sand samples around the Quilotoa volcano, in the Cotopaxi province, and four samples in some of the beaches of Santa Elena province; among them, Anconcito, Olón, and Montañita (see Figure 15). The first two samples were taken up from the southwest of the Quilotoa volcano, sampled from the surface. The second sample was collected from an intermittent fluvial environment with transporting volcanic pyroclastic flow in-origin particles. In the coastal area, it is known that some sands originated by the eroding process of the Chongón-Colonche Highlands delivering sediments onto Santa Elena province. Two sand samples were taken up from the high tide area of the Anconcito beach. The fifth sample was picked up from the high tide area of the Olón beach, and the sixth sample was obtained from the high tide area of the North of Montañita beach.



Figure 15: Sampling areas of the first field trip. (Map retrieved from Google maps)

In the second sampling field trip, carried out from July 30th to August 1st, 2018, the samples taken were originated by the erosion process of rocks from the Mache Chindul and Jama

Highlands, composed by mafic rocks marine in origin. One sand sample was collected from the Pedernales beach, in Manabí province, and other six from various beaches of the Esmeraldas province; among them: Río Verde, Tonsupa, Mompiche, and Punta Galera. (see Figure 16). First sand sample was collected from the high tide zone of the Río Verde beach. Samples 2 and 3 were taken up, respectively, from the high tide and low tide areas of the Tonsupa beach. The fourth sample was picked up from the high tide zone of the Pedernales beach. Samples 5 and 6 were obtained from the high tide area of the Mompiche beach, sample 6 was picked up from a mini mouth estuary zone. Sample 7 was taken up from the high tide area of the Punta Galera beach.



Figure 16: Sampling areas of the second fieldwork. (Source: Google maps)

6.1.2. Labeling

The labeling of the samples was carried out following the code shown in Figure 7. Based on this, each letter in each code has its meaning, that is:

The type of material is given by the letter **S** for Sand.

The province where the sampling was carried out is given by the letters:

X: Cotopaxi, **Y:** Santa Elena, **E:** Esmeraldas, and **M:** Manabí.

The sampling zone is denoted by the letters:

Q: Quilotoa, **A:** Anconcito, **O:** Olón, **M:** Montañita, **P:** Pedernales,

V: Rio Verde, **T:** Tonsupa, **M:** Mompiche, and **G:** Punta Galera.

Table 2 indicates the codification of each sand sample and the characteristics of the sampling.

Table 2: Natural sands information used to generate sample codification.

CODIFICATION	SAMPLING DATE	DESCRIPTION	SAMPLING ZONE
SXQ-101	16/07/2018	Iron-rich sands settled by volcanic eruptions taken from Quilotoa Volcano.	Cotopaxi, Southwest of Quilotoa volcano.
SXQ-102	16/07/2018	Iron-rich sands settled by volcanic eruptions, in an intermittent river environment, reworked from pyroclastic flows, taken from the Quilotoa Volcano.	Cotopaxi, Southwest of Quilotoa volcano.
SYA-103	17/07/2018	Beach sand collected in the high tide area of Anconcito.	Santa Elena, Anconcito Beach.
SYA-104	17/07/2018	Beach sand collected at the boundary between the high tide zone and the backshore in Anconcito.	Santa Elena, Anconcito Beach.
SYO-105	18/07/2018	Beach sand taken from the high tide area.	Santa Elena, Olón Beach.
SYM-106	18/07/2018	Beach sand taken from the high tide area.	Santa Elena, North of Montañita Beach.
SEV-201	30/07/2018	Silky Quartz sand collected in the high tide zone.	Esmeraldas, Río Verde. Upper part of the beach area.
SET-202	30/07/2018	Silky Quartz sand collected in the high tide zone	Esmeraldas, Tonsupa. Upper part of the beach area.
SET-203	30/07/2018	Silky Quartz sand collected in the low tide zone	Esmeraldas, Tonsupa. Upper part of the beach area.
SMP-204	31/07/2018	Micro-conglomerate sandy Quartz and Lithics taken from the high tide zone.	Manabí, Pedernales. Top of the beach.
SEM-205	31/07/2018	Quartz sand in the high tide zone.	Esmeraldas, Mompiche. Top of the beach.
SEM-206	31/07/2018	Quartz sand in the high tide zone.	Esmeraldas, Mompiche. Close to river mouth of a mini sandy estuary.
SEG-207	31/07/2018	Quartz sand in the high tide zone.	Esmeraldas, Punta Galera. Close to a bay.

6.1.3. Drying and Storing

The sand drying process was carried out in the University laboratory. Depending on the sand sample, this process took from 4 to 13 hours. Sand samples from Quilotoa volcano required less time to dry because, due to their volcanic origin, they were not saturated with water^{41,42}. On the other hand, sand samples collected from the Ecuadorian Coastal zone needed more hours to achieve a constancy in their mass. Sand samples SYO-105 and SEV-201 dried in 9 and 13 hours, respectively, which can be explained by its hydroponic environment by the presence of mangroves, the rapid rise of the tide^{43,44}. When losing the water, sands showed a lighter color (see Figure 17); also, the percentage of water lost, and the amount of water in the sands can be observed in the Annex B. Figure 18 indicates the dehydration of natural sand samples in respect of time. Samples SYO- 105 and SEV-201, which required more time to be dehydrated, are shown in the inset.



Figure 17: Comparison between wet (left) and dry (right) sand sample SET-203²⁶.

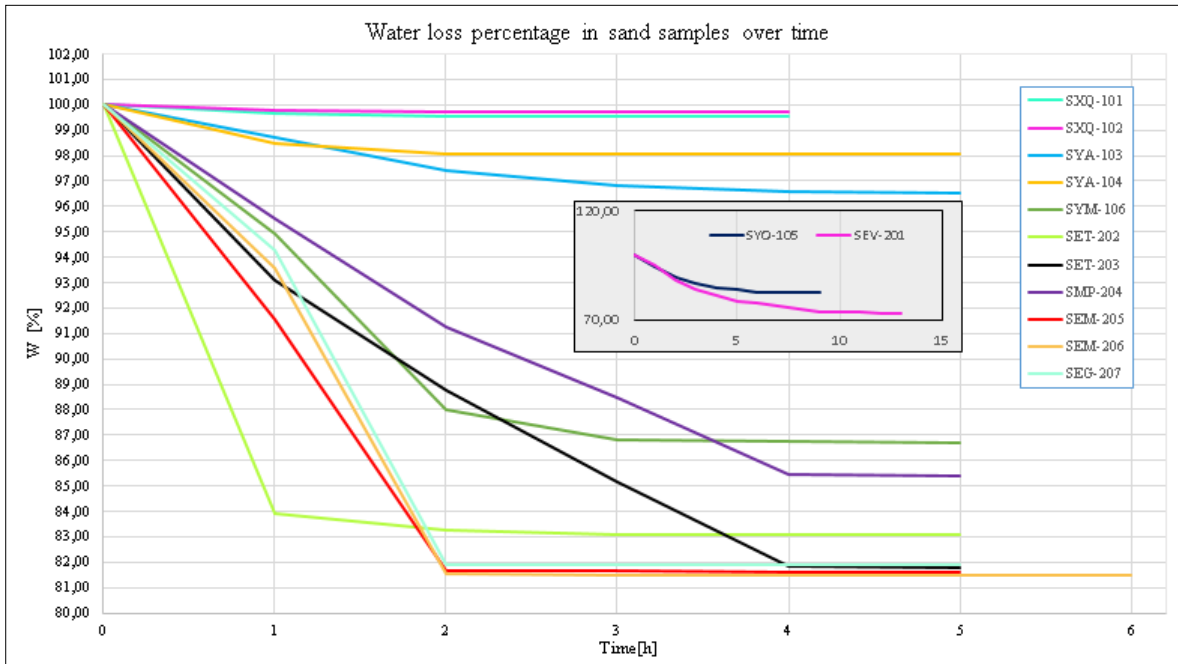


Figure 18: Water presence in natural sands

6.2. Characterization of natural sands

6.2.1. Dynamic Light Scattering

Dynamic Light Scattering (DLS) was performed to determine the particle size of the natural sand samples⁴⁵. Table 3 indicates: the particle size, surface area, and transmittance values of the thirteen sand samples. Also, as it shows, sample SXQ-102 has a lower particle size; therefore, its surface area presented is the major value⁴⁵.

Table 3: Particle size information of natural sands

Sample	Surface area (cm ² /cm ³)	Median size (µm)	Mean size (µm)	Transmittance /R (%)	Transmittance /B (%)
SXQ-101*	793.49	134.11	142.74	82.4	81.7
SXQ-102*	2623.70	95.12	98.98	84.0	85.1
SYA-103	163.54	383.07	548.90	86.5	89.4
SYA-104	179.36	349.74	558.64	85.1	88.4
SYO-105	308.89	176.57	756.65	80.5	85.8
SYM-106	218.19	257.12	747.29	88.9	91.7
SEV-201	1961.50	298.46	1364.26	81.5	76.7
SET-202	255.60	277.40	582.91	86.6	89.3
SET-203	278.89	219.45	480.00	87.3	89.6
SMP-204*	311.08	173.10	939.61	84.8	84.6
SEM-205	336.57	172.02	548.78	82.8	84.2

SEM-206	332.00	181.05	497.44	83.0	87.6
SEG-207	196.60	275.26	1202.55	86.0	88.3

*The size particle was bigger than the limit accepted by the device (1000 μm), so they were passed through an N° 100 sieve (size: 150 μm).

6.2.2. Atomic Absorption Spectrophotometry

This technique was used to measure the percentage concentration of iron in natural sand samples (See Annex C). The preparation of samples for AAS measurements can lead to do some errors, either because of the material used or because of the human⁴⁶. After the preparation of standard solutions, the obtained concentration values (see Table 4) were used to plot the calibration curve which gave the following equation:

$$A = 0.001175C_o + 0.02333$$

The resulting value for R^2 was 0.9873 which indicates a good linear correlation of the data.

Table 4: Iron concentration of standard solutions and absorbance

Concentration (ppm)	Absorbance
40	0.066
120	0.173
200	0.254

Table 5: Iron concentration of sample solutions and absorbance.

Sample	Iron Concentration (ppm) ± 7	Abs
SXQ-101	177	0.231
SXQ-102	155	0.206
SYA-103	103	0.144
SYA-104	121	0.165
SYO-105	30	0.058
SYM-106	114	0.157
SEV-201	79	0.116
SET-202	71	0.107
SET-203	57	0.09
SMP-204	104	0.146
SEM-205	95	0.135
SEM-206	73	0.109
SEG-207	95	0.135

Table 5 shows the values for concentration and absorbance of sample solutions with an error of 7, which was obtained by the formula:

$$S_{x_0} = \frac{S_{y/x}}{b} \sqrt{\frac{1}{n} + \frac{1}{m} + \frac{(y_0 - \bar{y})^2}{b^2(\sum(\bar{x} - x_0)^2)}} \quad (\text{Equation 4})$$

Where $S_{y/x}$ is the typical error of the equation, b is the intercept, n is the number of measurements (in this case, it was 1), m is the number of standard solution concentration values, y is the absorbance, and x is the concentration. Then the percentage concentration of iron in samples was determined by the formula:

$$\%Fe = C_o \left(\frac{mg}{L} \right) \cdot \frac{V_o(L)}{m_{(diluted\ sample)}(mg)} \cdot \left(\frac{V_{flask}(mL)}{V_{aliquot}(mL)} \right)^* \cdot 100 \quad (\text{Equation 5})$$

**Samples that presented a concentration higher than standard values were diluted to lower concentrations.*

In order to have all concentrations within the calibration curve, samples that presented very high concentrations were diluted. For samples SXQ-102 and SYA-104, the sample solution was diluted to 25 %, so $V_{aliquot}(mL) = 25$; in the case of SYM-106 and SEV-201, the sample solution was diluted to 50 %, so $V_{aliquot}(mL) = 50$.

The error associated with the concentration of iron in the sample was denoted by:

$$S_c = \sqrt{\left(\frac{S_m}{m}\right)^2 + \left(\frac{S_v}{v}\right)^2 + \left(\frac{S_a}{a}\right)^{2*} + \left(\frac{S_{C_o}}{C_o}\right)^2}$$

Where, S is the error associated with the instrument used to measure mass (m), volume (v), aliquot (a), and S_{C_o} is the error associated with the concentration given by the software (C_o).

Then, Figure 19 shows that, sand samples SXQ-102 and SYA-104, presented the highest concentration of Fe, 17.9 ± 0.7 % Fe and 13.2 ± 0.7 % Fe, respectively.

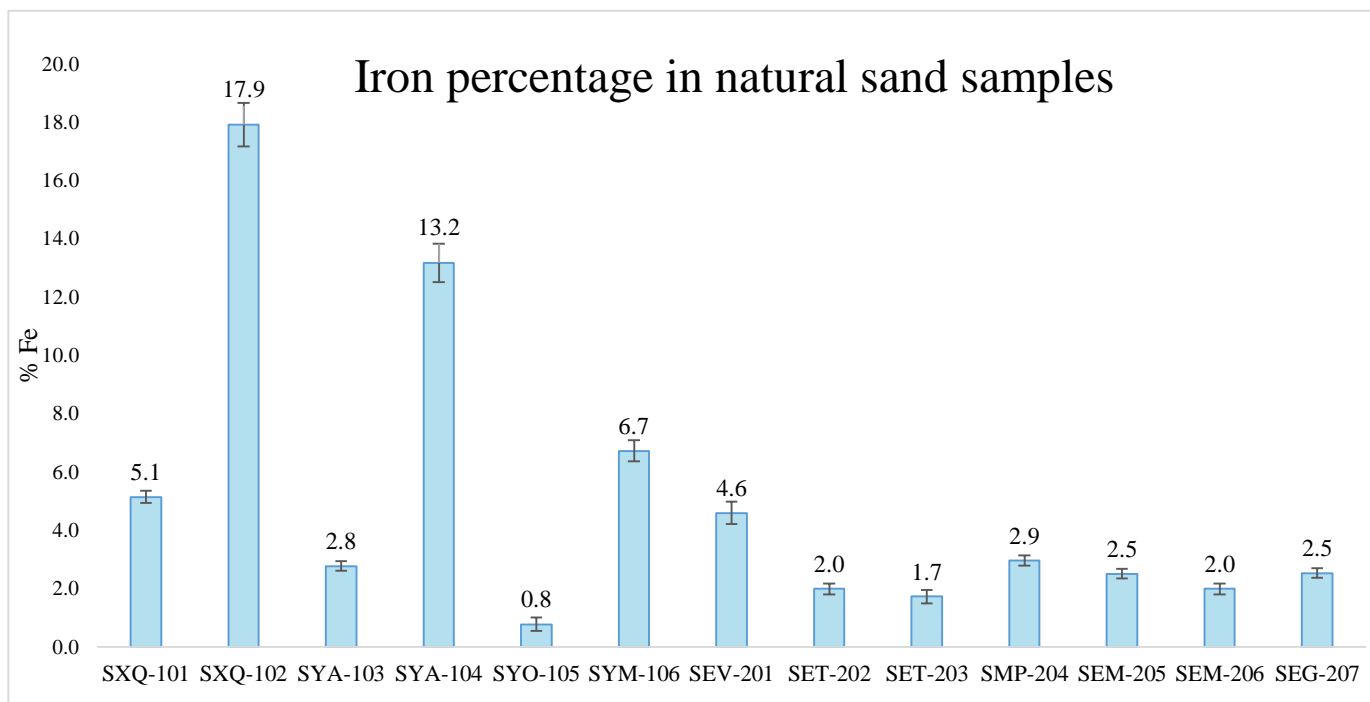


Figure 19: Iron percentage in natural sand samples determined by applying the AAS.

6.2.3. Energy Dispersive Spectroscopy

The estimated chemical composition of natural sand samples was analyzed by SEM-EDS technique. Table 6 indicates the semi-quantitative analysis of natural sands expressed as oxides. In sand samples SYA-103 and SYA-104, the presence of potassium oxides was too low that it was neglected by the software. The same thing happened to SYO-105 with magnesium oxides. This analysis also showed that samples SXQ-102 and SYA-104 contain the major amount of iron and, along with SEM-205, they present the highest concentration of titanium oxides.

Table 6: Chemical semi-quantitative composition of sand sample, expressed in oxides, by SEM-EDS analysis.

Samples/Oxides	Na	Mg	Al	Si	K	Ca	Ti	Fe
SXQ-101	5.27	2.19	17.86	61.65	1.47	5.43	0.59	5.56
SXQ-102	4.55	1.80	15.88	58.32	1.58	4.61	1.42	11.84
SYA-103	1.42	1.37	3.82	44.10	0*	47.27	0.15	1.87
SYA-104	1.74	3.30	5.67	53.99	0*	27.15	1.25	6.91
SYO-105	3.52	0*	10.08	72.68	0.81	10.66	0.33	1.92
SYM-106	3.24	1.35	9.13	72.20	0.91	10.84	0.30	2.04
SEV-201	3.82	3.11	18.25	62.04	1.53	4.51	0.58	6.17
SET-202	3.77	1.90	11.79	64.44	0.93	13.88	0.21	3.09
SET-203	3.54	2.27	11.23	58.75	0.98	19.29	0.36	3.60
SMP-204	3.69	2.54	13.54	62.53	1.29	9.88	0.63	5.90

SEM-205	4.71	1.93	15.71	64.08	1.00	6.49	1.56	4.52
SEM-206	4.64	1.51	15.27	68.51	0.83	6.27	0.44	2.54
SEG-207	3.78	2.12	12.35	68.97	g	7.84	0.38	3.54

*Value, between 0-0.5, negligible to be considered.

6.2.4. X-Ray Diffraction

Measurements of natural sand samples with XRD were performed by the powder method. The results were analyzed by using QualX2 software along with its search and match options. Then, database file entries were obtained from Crystallography Open Database (COD)⁴⁷⁻⁵⁰. Figure 20 Figure 21 below show the X-ray diffraction patterns of the natural sand samples on which the study was based on. X-ray diffraction patterns of all natural sand samples are found in Annex D.

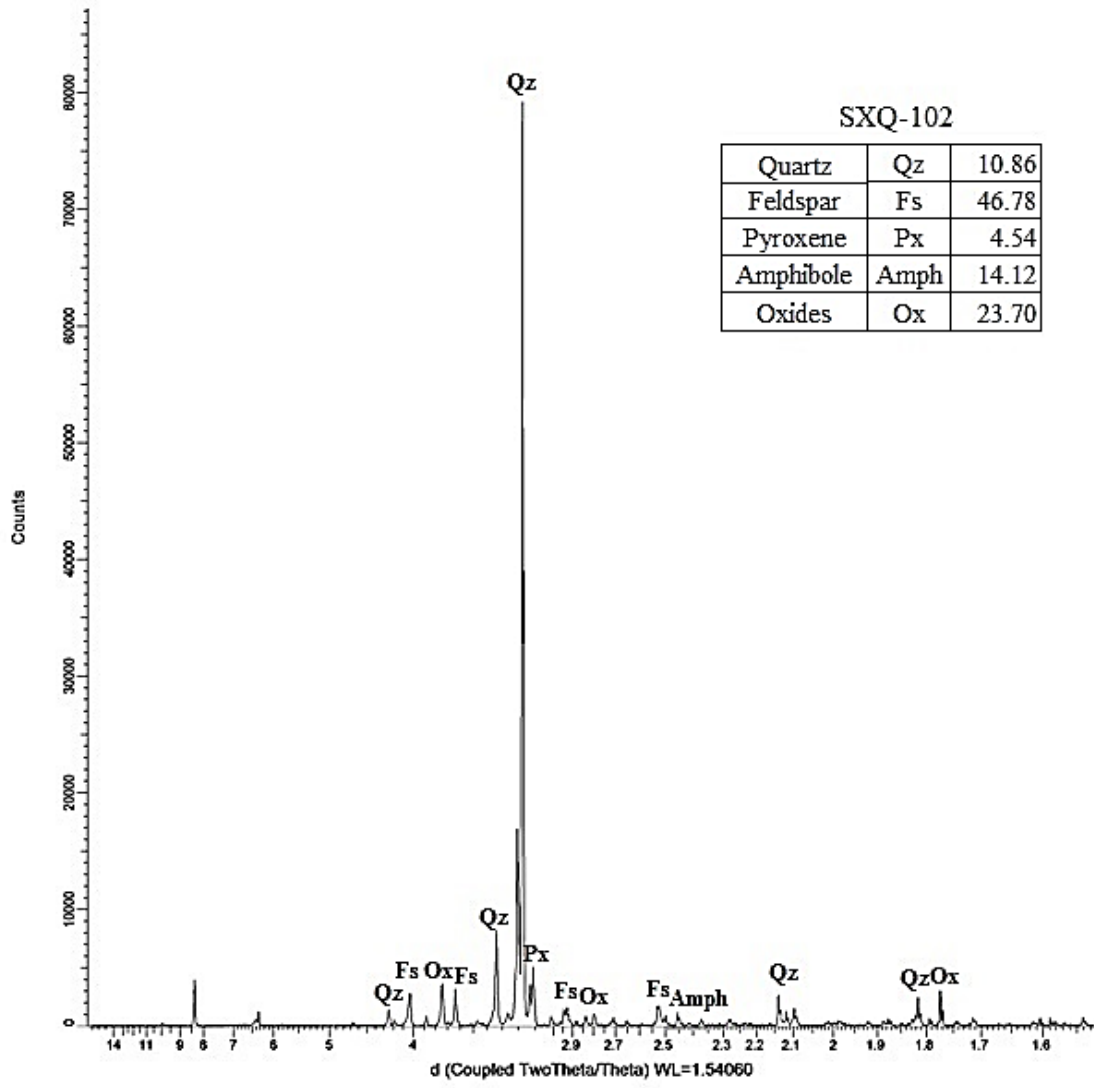


Figure 20: X-ray diffraction pattern of SXQ-102 sample. Included the percentage table of mineral phases present in the sample: Quartz (Qz), Feldspar (Fs), Pyroxene (Px), Amphibole (Amph), and Oxides (Ox).

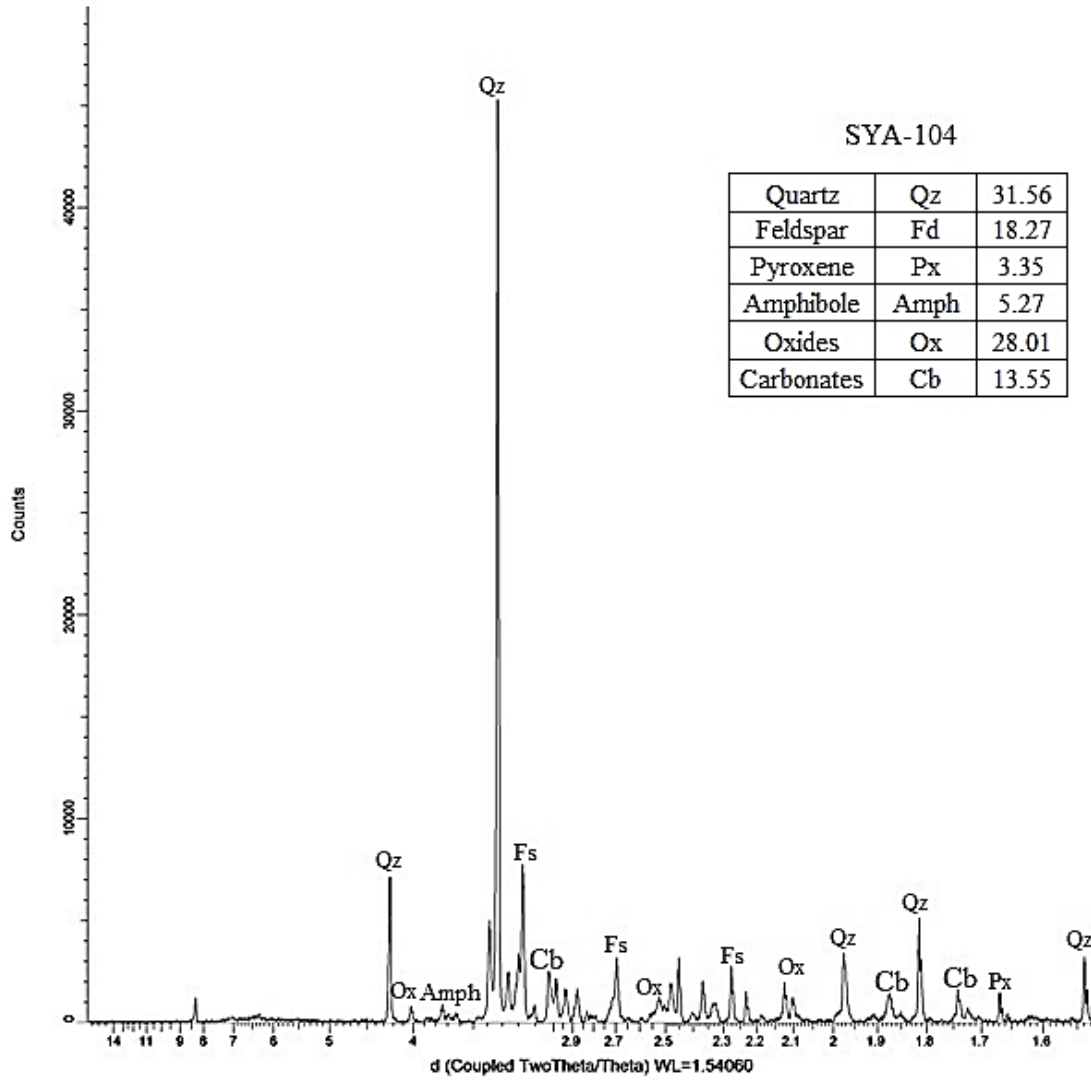


Figure 21: X-ray diffraction pattern of SYA-104. Included the percentage table of mineral phases present in the sample: Quartz (Qz), Feldspars (Fs), Pyroxenes (Px), Amphiboles (Amph), Oxides (Ox), and Carbonates(Cb)

Table 7: Mineral phases of natural sands.

Card COD	Compound name	Chemical formula	Sample name												
			SXQ-101	SXQ-102	SYA-103	SYA-104	SYO-105	SYM-106	SEV-201	SET-202	SET-203	SMP-204	SEM-205	SEM-206	SEG-207
Silica Polymorphs			7,90	10,86	29,16	31,56	30,80	32,59	12,90	32,94	46,60	27,50	4,13	30,77	33,53
00-101-1159	Quartz low	SiO ₂	3,95	2,64	0,33	-	0,39	-	-	-	0,90	0,60	4,01	19,44	29,31
00-900-9666	Quartz	SiO ₂	3,59	8,09	28,18	31,56	30,40	30,00	12,90	29,76	45,70	26,90	0,07	9,31	3,14
00-900-9685	Cristobalite	SiO ₂	0,36	0,13	0,65	-	-	2,59	-	3,18	-	-	0,05	2,01	1,08
Feldspars			46,93	46,78	16,02	18,27	42,92	48,62	75,40	43,98	33,00	53,70	35,04	27,40	24,76
00-900-0702	Albite	AlNaO ₈ Si ₃	14,69	18,59	-	10,39	-	-	35,00	-	6,90	6,60	-	13,36	-
00-901-1423	Oligoclase	Al _{1,277} Ca _{0,277} Na _{0,723} O ₈ Si _{2,723}	13,59	-	-	-	16,65	-	10,50	10,11	-	-	-	-	-
00-210-8010	Andesine	Al _{1,44} Ca _{0,49} Na _{0,51} O ₈ Si _{2,56}	18,65	28,19	-	-	-	-	-	-	-	-	-	-	-
00-900-0744	Labradorite	Al _{0,81} Ca _{0,325} Na _{0,16} O ₄ Si _{1,19}	-	-	16,02	-	4,00	15,91	22,20	-	13,90	31,10	28,55	14,04	14,72
00-901-1200	Bytownite	Al _{0,92} Ca _{0,43} Na _{0,07} O ₄ Si _{1,08}	-	-	-	7,88	9,07	32,72	-	21,02	12,20	-	6,49	-	10,04
00-900-1260	Anorthite	AlCa ₄ Si	-	-	-	-	-	7,70	12,85	-	16,00	-	-	-	-
00-900-5308	Microcline	KAlSi ₃ O ₈	-	-	-	-	13,19	-	-	-	-	-	-	-	-
Pyroxenes			38,96	4,54	6,96	3,35	3,04	8,57	1,30	4,20	4,00	12,20	34,55	10,84	29,79
00-901-3275	Aegirine	NaAlSi ₃ O ₆	-	-	-	0,28	3,04	-	-	-	3,10	1,10	4,81	4,23	-
00-900-0800	Diopside	CaMgO ₆ Si ₂	-	4,54	1,94	-	-	-	1,30	-	0,90	-	-	-	-
00-900-2907	Pyroxene	CaMgO ₆ Si ₂	-	-	-	-	-	5,25	-	-	-	1,90	1,51	-	6,24
00-100-0047	Enstatite	Mg ₂ (Si ₂ O ₆)	38,96	-	5,02	-	-	-	-	-	-	-	28,24	-	23,56
00-900-4084	Omphacite	Al _{0,51} Ca _{0,5} Fe _{0,06} Mg _{0,46} Na _{0,5} O ₆ Si _{1,97}	-	-	-	3,07	-	-	-	4,20	-	-	-	-	-
00-900-354	Pigeonite	Fe _{0,01} Ti _{0,01} Ca _{0,01} Si ₂ Al _{0,02} Mg _{0,23} Na _{0,001} O ₆	--	-	-	-	-	3,32	-	-	-	9,20	-	6,61	-
Amphiboles			4,88	14,12	20,53	5,27	5,07	4,42	4,00	6,90	0,00	0,00	0,82	19,20	2,81
00-900-4433	Hornblende	Fe _{0,29} Ti _{0,07} Ca _{1,81} Si _{4,88} AlMg _{0,38} Na _{0,14} O ₂₄ H _{1,78}	4,88	4,99	10,57	5,27	-	4,42	4,00	6,90	-	-	0,82	19,20	2,81

00-900-0300	Epidote	$Al_{2,6}Ca_2Fe_{0,4}HO_{13}Si_3$	0,00	9,14	9,96	-	5,07	-	-	-	-	-	-	-	-
Oxides			1,33	23,70	14,53	28,01	15,07	5,79	6,40	3,55	5,10	3,50	25,40	11,47	9,01
00-900-7644	Magnetite	Fe_3O_4	0,31	0,12	-	11,3	-	-	-	-	-	-	-	-	0,795
00-210-8028	Hematite	Fe_2O_3	-	15,50	-	0,65	-	-	-	-	0,60	-	-	3,95	-
00-900-0911	Ilmenite	FeO_3Ti	-	7,74	1,80	0,22	-	-	-	-	-	-	1,73	5,17	8,12
00-900-1629	Ferrosilite	$FeSiO_3$	-	-	-	9,10	4,17	0,86	-	2,35	-	-	-	-	-
00-153-2800	Iron Oxide	Fe_2O_3	1,02	0,16	1,04	0,05	-	-	-	-	0,40	-	6,22	-	0,08
00-900-8196	Titanium Oxide	Ti_4O_7	-	-	-	4,96	10,90	4,94	-	-	4,10	3,50	-	-	-
00-900-1874	Titanite	$CaTiSiO_5$	-	0,17	11,69	1,72	-	-	6,40	1,20	-	-	0,11	2,35	0,02
00-231-0618	Calcium Titanate	$CaTiO_3$	-	-	-	-	-	-	-	-	-	-	17,34	-	-
Carbonates			0,00	0,00	12,80	13,55	3,11	0,00	0,00	8,44	8,80	3,10	0,06	0,31	0,10
00-101-0928	Calcite	$CaCO_3$	-	-	0,65	13,55	3,11	-	-	2,04	8,80	3,10	-	0,31	0,10
00- 900-0083	Dolomite	$CaMg(CO_3)_2$	-	-	0,29	-	-	-	-	-	-	-	-	-	-
00-900-0229	Aragonite	$CaCO_3$	-	-	11,86	-	-	-	-	6,40	-	-	0,06	-	-
Mafics			0,00	0,00	0,00	0,00	0,00	0,00	0,00	0,00	2,50	0,00	0,00	0,00	0,00
00-900-1096	Olivine	Mg_2O_4Si	-	-	-	-	-	-	-	-	2,50	-	-	-	-

The semi-quantitative mineral composition of all natural sand samples was provided by QualX2 software by using the Crystallographic Open Database (COD)⁴⁷. Mineral phases were matched according to their mineral group. Silica polymorph group presents the subgroups quartz, quartz low and cristobalite which are silicon oxide (SiO₂) minerals. Feldspar group presents the minerals albite, oligoclase, andesine, labradorite, bytownite, anorthite, and microcline; those are composed of aluminosilicates. Pyroxene group presents the minerals aegirine, diopside, pyroxene-ideal, enstatite, omphacite, and pigeonite. Hornblende and epidote are assigned in the amphibole group. In the group of oxides are magnetite, ilmenite, hematite, ferrosilite, and other iron and titanium oxides. In the carbonates group are calcite, aragonite, and dolomite. Mafic minerals were also found in samples, which is the case of Olivine. According to the results obtained by the SEM-EDS analysis, it was expected to observe approximately more than 50% SiO₂; however, it oscillates from 4% to 45% of the total composition of the natural sand samples. Table 7 indicates the chemical composition of mineral assigned to the diffractometer signals. As it shows, feldspar, pyroxene, and amphibole minerals are composed of silicon oxides which explain the elevated amounts of silicon and aluminum oxides obtained by the EDS analysis (see Table 6). Besides, Figure 20 and Figure 21 show that major counts of minerals present in natural sand sample SXQ-102 and SYA-104 are Quartz (SiO₂).

6.3. Reactivity

Based on the results obtained after the characterization of natural sands through DLS, AAS, EDS, and XRD, the best candidates chosen for the sands reactivity with hydrogen sulfide are SXQ-102 and SYA-104 because those samples present the higher concentration of iron and titanium oxides in their composition.

6.3.1. Enrichment of natural sands

Magnetic separation was done by using a magnet coated with plastic in wet media. Magnetic grains were attached to the magnet along with some small grains (see Figure 22). When the separation was done, the enriched sand was dried at 90°C for 12 hours and weighted to calculate the percentage of magnetic mineral content from the total mass of the sample. The percentage was obtained by using Equation 3:

$$\%E(SXQ - 102) = \frac{80.95}{250g} * 100 = 32.38\%$$

$$\%E(SYA - 104) = \frac{22.73}{250g} * 100 = 9.09\%$$

The percentage of magnetic minerals of sand samples were 32.38% SXQ-102, and 9.09% SYA-104. Sand sample from Quilotoa volcano presented a higher yield because the sand taken to be enriched was previously sieved. These yield values indicate the amount of sand obtained after the enrichment. For sand sample SXQ-102, this value can be justified because, for this process, it was taken a quarter part of the sieved sample.

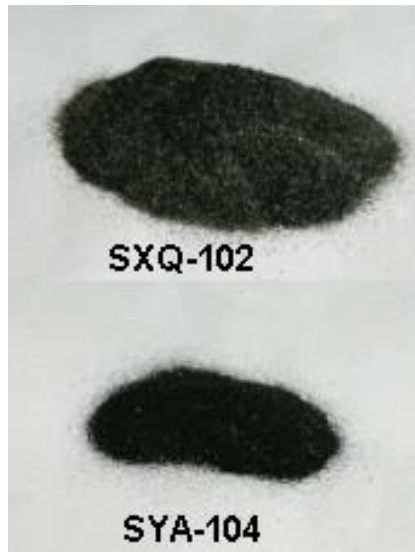


Figure 22: Enriched black sands.

6.3.2. Characterization of enriched black sands

6.3.2.1. Dynamic Light Scattering for enriched sands

Values of particle size and surface area of enriched sands are shown in Table 8. Sample SYA-104 presents a bigger surface area than SXQ-102, so it is expected that the contact area of the particle will allow better adsorption of the gas.

Table 8: Particle size data about enriched sands

Sample	Surface Area	Median size (µm)	Mean size (µm)	Transmittance /R (%)	Transmittance /B (%)
SXQ-102	225.78	277.51	291.68	88	77.2
SYA-104	305.90	195.63	570.21	90.3	91.9

6.3.2.2. Atomic Absorption Spectrophotometry for enriched sands

First, concentration values for standard solutions were used to plot the calibration curve for enriched sands. The value for R^2 was 0,9949, and the resulting equation was:

$$A = 0,0175000 C_o + 0,0012125$$

Where A is the Absorbance and C_o is the Concentration.

Then, this equation was used to determine the standard error associated with the percentage iron concentration of enriched sands. The results obtained by atomic absorption analysis in enriched sands revealed the highest iron content of 56.7 ± 0.2 % Fe in sample SXQ-102, and the lowest iron concentration of 42.8 ± 0.2 % Fe in sample SYA-104 (see Figure 23).

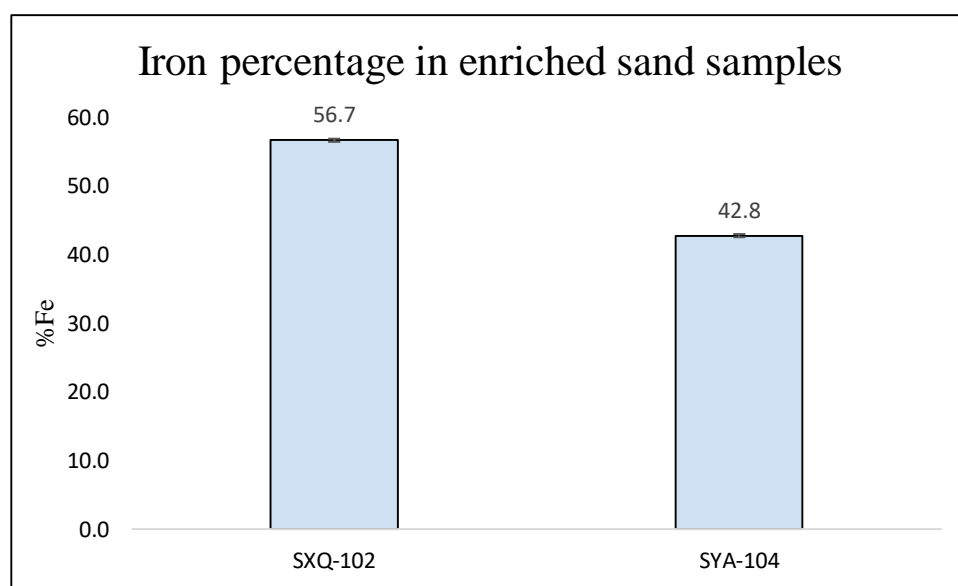


Figure 23: Iron percentage in enriched sands by AAS.

6.3.2.3. Energy Dispersive Spectroscopy for enriched sands

The chemical composition of enriched sands expressed in oxides is shown in Table 9. Here, the enrichment of sands is demonstrated in the elevated percentage of iron and titanium oxides concerning the other oxides. This semi-quantitative analysis reveals that sample SXQ-102 has more concentration of iron oxide; while sample SYA-104 presents a higher amount of titanium oxides.

Table 9: Chemical composition of enriched sands by SEM-EDS analysis, expressed as oxides.

Enriched Sands							
Sample/Oxide	Na	Mg	Al	Si	Ca	Ti	Fe
SXQ-102	2.86	2.52	8.06	25.53	1.99	7.20	51.84
SYA-104	1.63	8.83	5.15	21.12	2.42	12.30	48.54

6.3.2.4. X-Ray Diffraction for enriched sands

The semi-quantitative analysis of the mineral phases present in enriched sands (see Table 10) indicates that sample SXQ-102 has a majority mineral phase that is magnetite; while in the case of sample SYA-104, the majority mineral phase is ilmenite. Also, Al, Si, Na, Ca are found in enriched sands in the form of quartz and feldspars minerals

Table 10: Mineral phases present in enriched sands by XRD analysis

COD card	Compound	Chemical formula	Sample	
			SXQ-102	SYA-104
00-101-1084	Magnetite	Fe ₃ O ₄	34.13	11.88
00-210-8028	Hematite	Fe ₂ O ₃	16.09	3.99
00-900-0911	Ilmenite	FeO ₃ Ti	18.74	62.62
00-153-2800	Iron Oxide	Fe ₃ O ₄	14.36	0.38
00-900-9666	Quartz	SiO ₂	2.70	0.70
00-900-1874	Titanite	CaTi SiO ₅	-	2.80
00-900-1629	Ferrosilite	FeSiO ₃	-	12.34
00-900-0525	Feldspar	AlNaO ₈ Si ₃	13.99	5.28

Figure 24 and Figure 25 indicate the diffraction pattern of enriched sands, these show the mineral phases present in the enriched sand samples, where: M refers to magnetite, H to hematite, I to ilmenite, F to iron oxides, T to titanite, Qz to quartz, Fs to feldspar, and Fsi to ferrosilite. The concentration of quartz and feldspars in the sample is due to the small particles of silica dragged by the magnetic particles during the magnetic enrichment. In here, magnetite mineral phase presents most counts than the other mineral phases, in sand sample SYA-104 (see Figure 25), the ilmenite phase has more counts than in the sample SXQ-102 (see Figure 24) which explains the elevated concentration of titanium in sand sample SYA-104 observed by SEM-EDS (see Table 1).

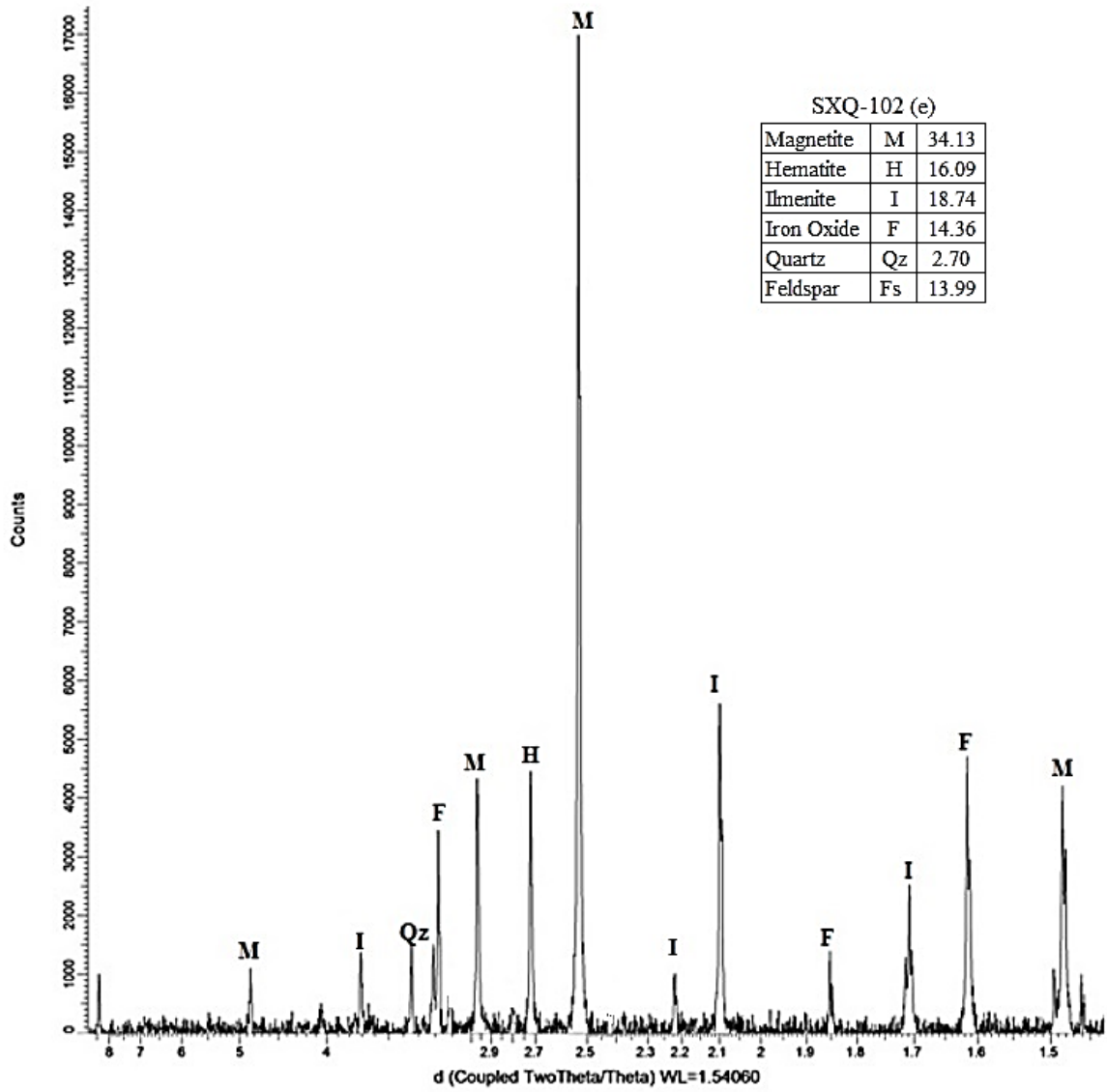


Figure 24: X-ray diffraction pattern for enriched black sand sample SXQ-102. The inset includes the percentage of mineral phases in the sample.

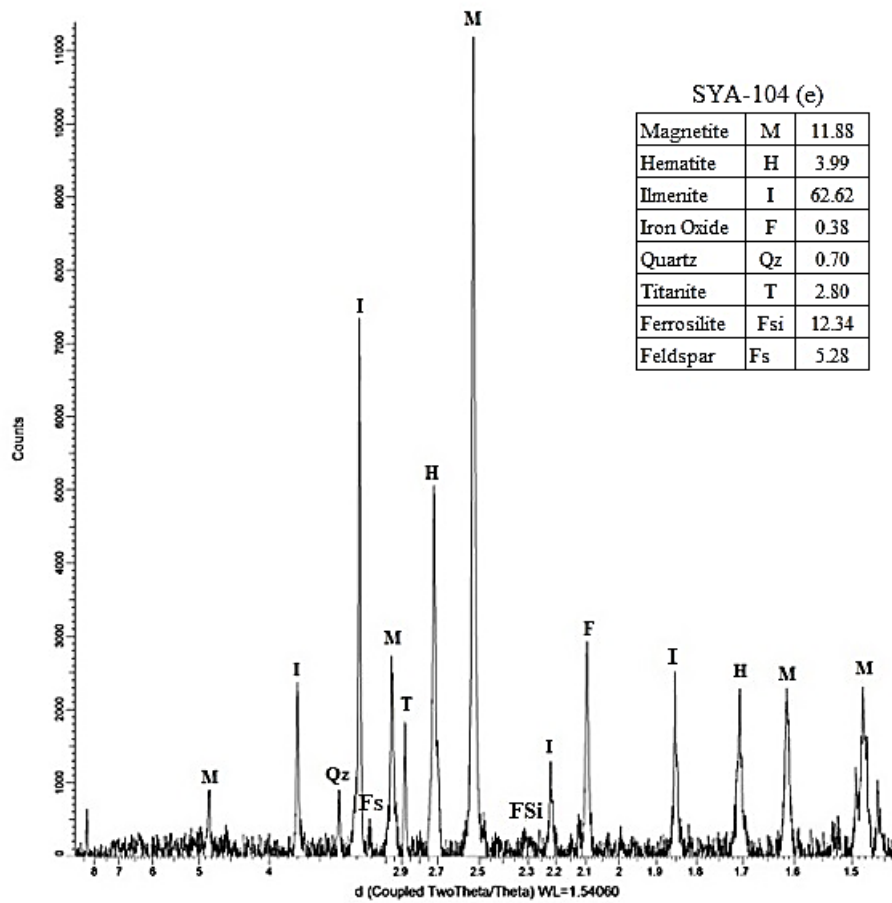


Figure 25: X-ray diffraction pattern for enriched black sand sample SYA-104. The inset includes the percentage of mineral phases in the sample.

6.3.3. Reactivity of enriched black sands

The system used in the reactivity of sands is shown in Figure 26. The acid gas was generated through the exothermic reaction of iron(II) sulfide in hydrochloric acid (see Equation 1). After two weeks of reactivity, the sands presented a change in their color, from black to greenish

yellow; also, the sand looked moistened (See Figure 27). As a result of the reactivity of the black sands with H_2S , some possible chemical reactions can be obtained⁵, among them are:²⁶

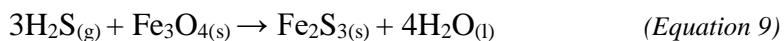
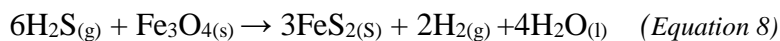
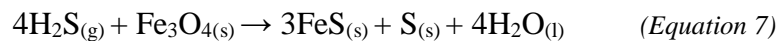
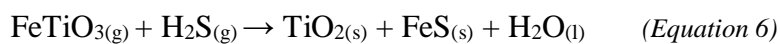


Figure 26: Reactivity setup

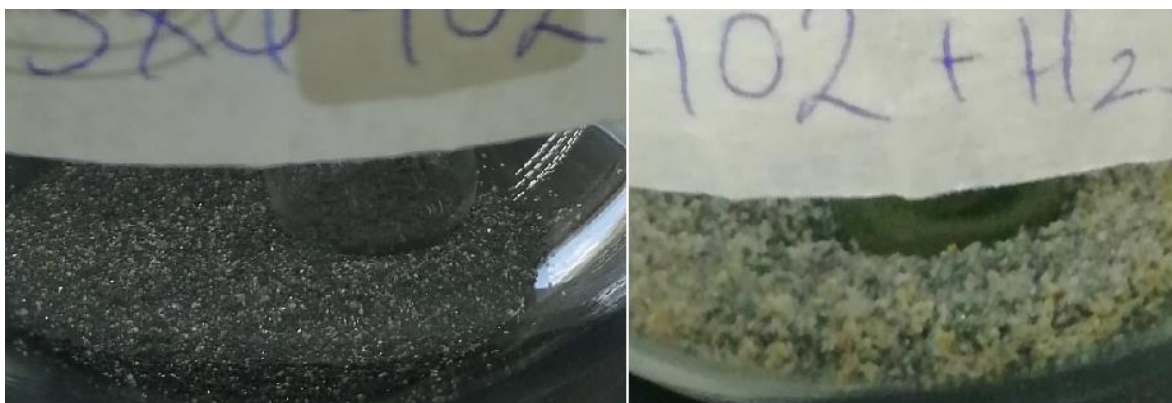


Figure 27: Black sand sample SXQ-102 before (left) and after (right) reacting with Hydrogen Sulfide.

6.3.4. Characterization of reacted black sands

6.3.4.1. pH Test of reacted sands

The pH of reacted sands was compared with that of enriched sands. As a result, enriched sands presented a neutral pH (7) before the reactivity, and it was acid (2-3) after the reactivity with hydrogen sulfide (see Figure 28). The change in the acidity of the sand indicates that it was affected by the presence of sulfide ions on the surface of the particle. When diluted, H^+ ions reacted with sulfur(S), lowering the pH of the soil⁵².

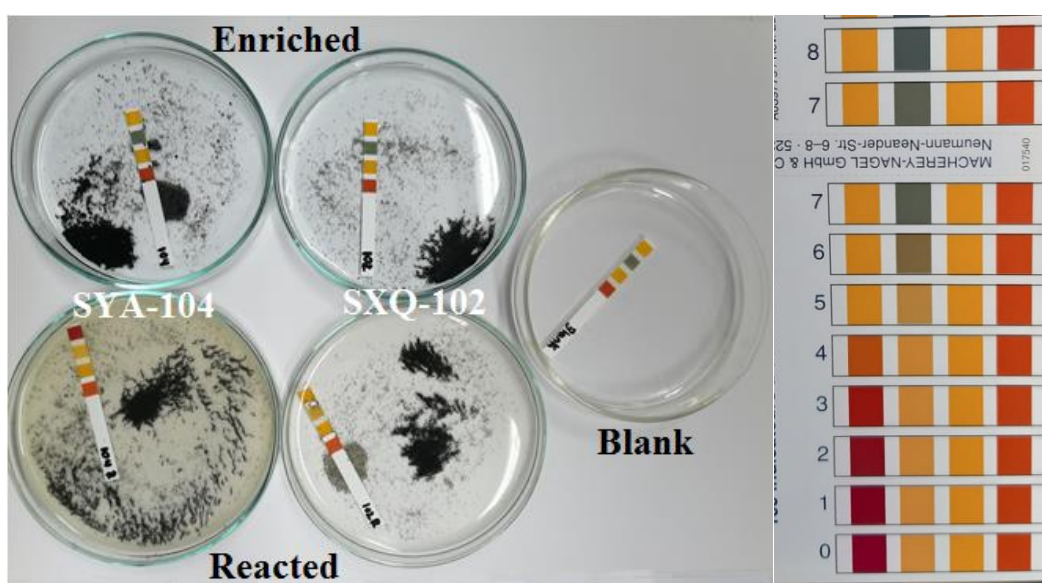


Figure 28: pH test results. Enriched sands: pH 7; Reacted sands: pH 3 (SXQ-102), and pH 2 (SYA-104)

6.3.4.2. Energy Dispersive Spectroscopy for reacted sands

The semi-quantitative chemical composition of reacted sands by SEM-EDS technique is shown in Table 11. In this analysis, it can be observed that sulfur and chlorine appears. Sulfur confirms the reactivity of the sands with the gas H_2S , sample SYA-104 shows to have adsorbed more sulfur than sample SXQ-102. On the other hand, the presence of chlorine can be explained by the presence of fumes of hydrochloric acid (HCl) in the reactivity setup for the generation of hydrogen sulfide (H_2S).

Table 11: Chemical composition of reacted sands by SEM-EDS analysis

Reacted sands										
Sample/Elemental*	Na	Mg	Al	Si	S	Cl	Ca	Ti	Fe	Total
SXQ-102	2.36	1.75	5.69	16.34	3.92	18.26	2.00	4.11	45.56	100.00
SYA-104	0.91	4.49	3.12	10.44	12.88	7.06	2.21	8.63	50.26	100.00

*EDS elemental analysis for reacted sands was realized to observe the presence of atoms in form of elements, in order to find sulfur.

6.3.4.3. X-Ray Diffraction for reacted sands

The X-ray diffraction analysis of reacted sands showed the presence of ilmenite, magnetite, hematite, iron oxide, quartz, and feldspar; and also it indicates the presence of iron and titanium sulfides (see Table 12). The X-ray diffraction patterns for reacted sand sample SXQ-102 (see Figure 29), and SYA-104 (see Figure 30) was compared to enriched black sands diffraction patterns (see Figure 24 Figure 25), and the presence of new peaks showed that, in effect, black sand samples reacted with sulfur. The analysis of the X-ray diffraction patterns, by using Qualx2 Software, revealed that new peaks appeared which belonged to iron sulfide, titanium sulfate and titanium oxide (as expected in Equations 6, 7, 8, and 9). Enriched black sand sample SYA-104 presented higher ilmenite (FeTiO_3) content; for this reason, the reacted sand shows titanium oxide and titanium sulfate as products (see Equation 6).

Table 12: Mineral phases of reacted sands

COD card	Compound name	Chemical formula	Abundance [%] / Sample	
			SXQ-102	SYA-104
00-901-0914	Ilmenite	FeO_3Ti	7.31	31.16
00-101-1084	Magnetite	Fe_3O_4	34.51	14.64
00-210-8028	Hematite	Fe_2O_3	7.53	0.24
00-153-2796	Iron oxide	Fe_3O_4	13.32	1.99
00-900-9666	Quartz	Si O_2	5.52	3.52
00-500-0115	Iron sulfide (Pyrite)	FeS_2	13.07	1.59
00-900-0525	Feldspar	$\text{Al}_{0.81}\text{Ca}_{0.325}\text{Na}_{0.16}\text{O}_4\text{Si}_{1.19}$	18.75	16.45
00-210-0942	Titanium sulfate	$\text{Ti S}_2\text{O}_8$	-	20.51
00-100-8201	Titanium oxide	Ti_6O_{11}	-	9.90

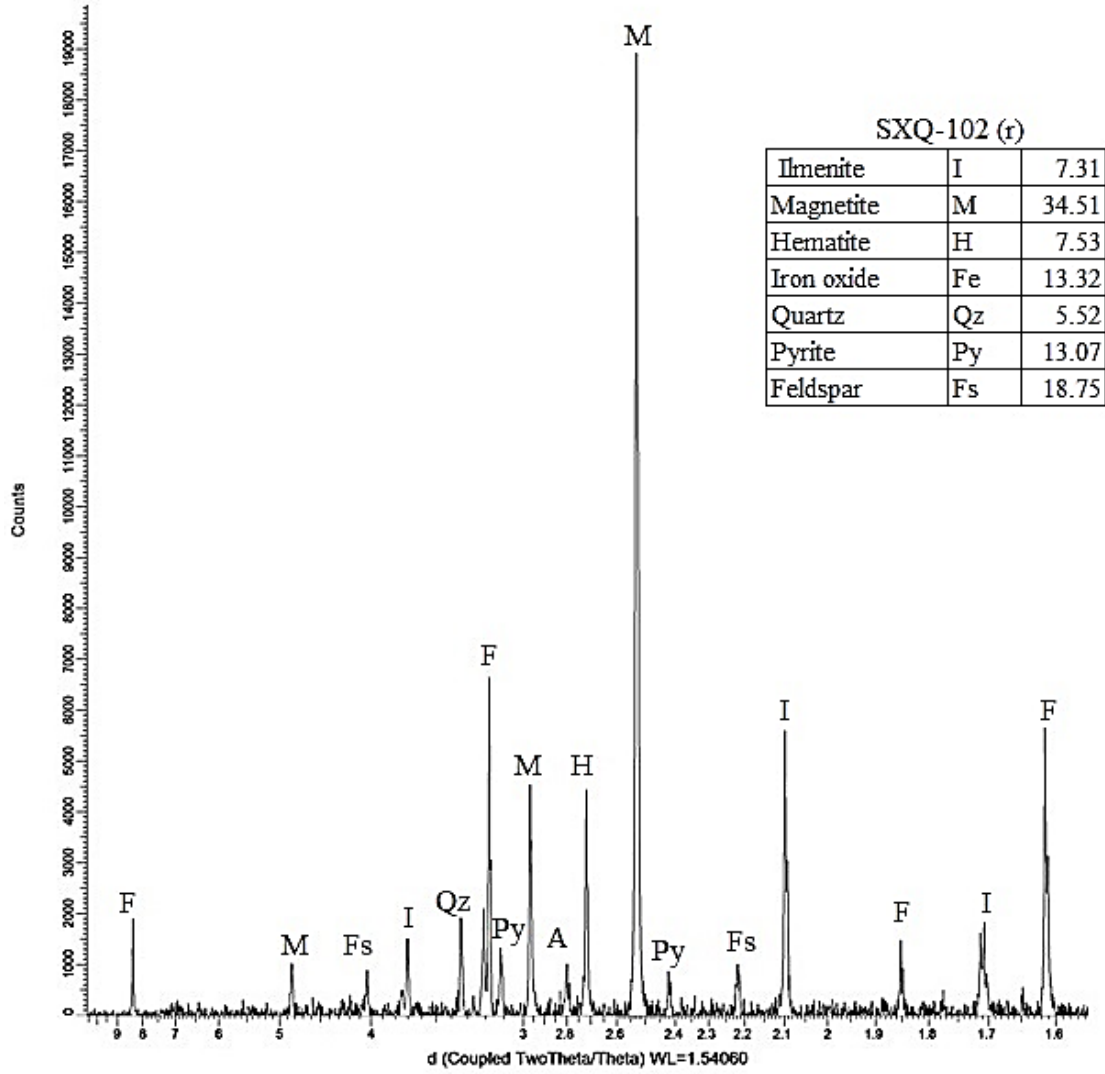


Figure 29: X-ray diffraction pattern for reacted sand sample SXQ-102. The inset includes the percentage of mineral phases in the sample.

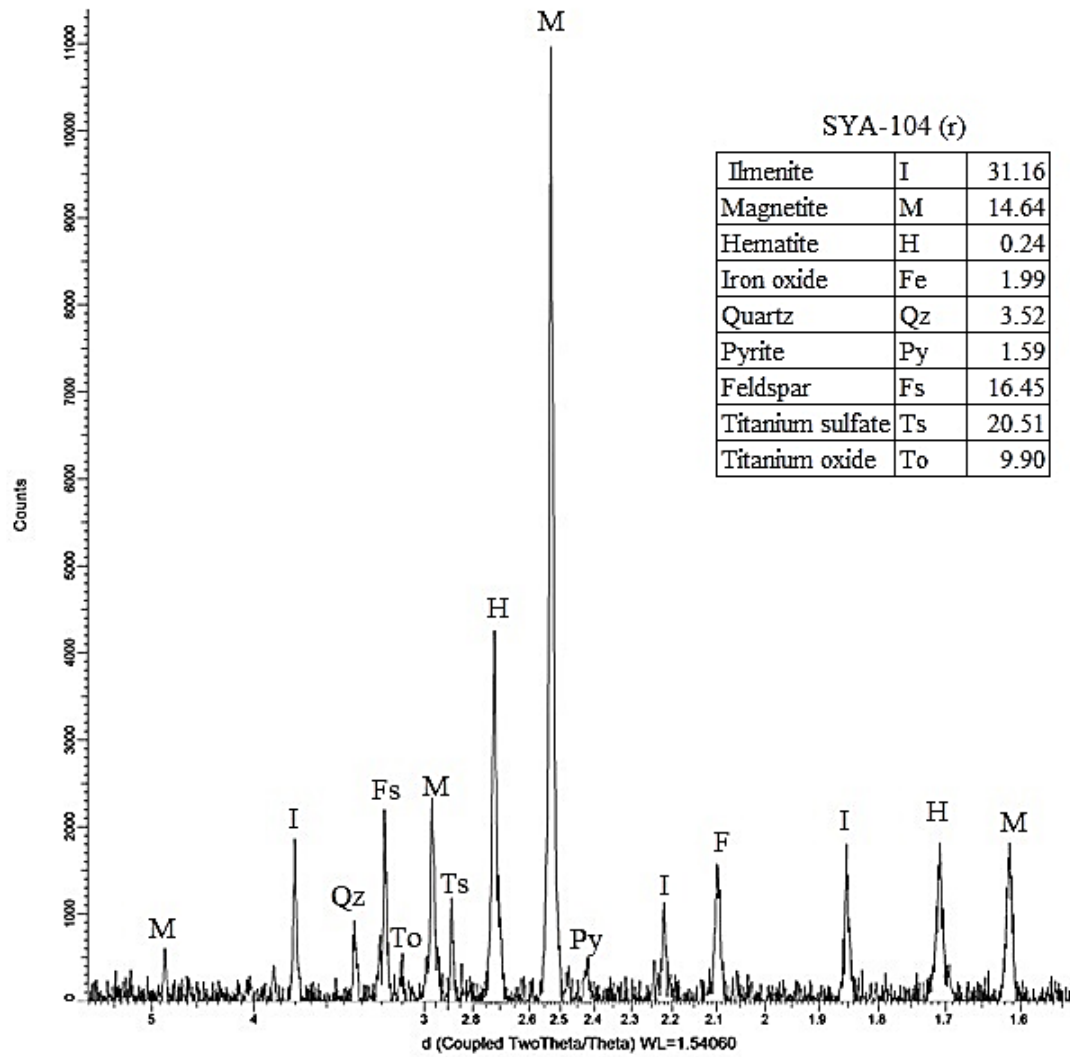


Figure 30: X-ray diffraction pattern for reacted sand sample SYA-104. The inset includes the percentage of mineral phases in the sample.

CHAPTER VII: CONCLUSIONS AND RECOMMENDATIONS

7.1. Conclusions

- Thirteen unconsolidated black sand samples were collected from different areas of Ecuador, among them Quilotoa in Cotopaxi province; Anconcito, Olón and Montañita in Santa Elena province; Río Verde, Tonsupa, Mompiche and Punta Galera in Esmeraldas province, and Pedernales in Manabí.
- The characterization of natural sand samples, by using Dynamic Light Scattering (DLS), indicated that sample SXQ-102 had a bigger surface area. This data reveals the high adsorption capacity of their particles which makes it a possible good candidate for reactivity with H₂S for natural gas sweetening processes.
- The Atomic Absorption Spectrophotometry (AAS), carried out to determine the concentration of iron in the samples, revealed that samples SXQ-102 and SYA-104 presented a higher amount of iron in their composition, 17.9 ± 0.7 % Fe and 13.2 ± 0.7 % Fe, respectively.
- Energy Dispersive Spectroscopy provided a semi-quantitative analysis of the composition of natural sands which showed the presence of Si, Al, Na, Mg, Ca, K, Ti, and Fe oxides. Samples with the highest percentage of iron and titanium oxides in their composition were SXQ-102 and SYA-104, with 11.84 % Fe and 1.42 % Ti, and 6.91 % Fe and 1.25 % Ti respectively. Mostly, a high amount of silicon oxide was found.
- The mineral phases present in sand samples were identified through X-Ray Diffraction (XRD). The majority of minerals, in almost all samples, present silicon oxide, which appears in the analysis as: quartz, feldspars, pyroxenes, and amphiboles minerals. Then, iron and titanium oxides represent a low percentage in the samples respect to silicon oxides.
- The magnetic enrichment of natural sand samples SXQ-102 and SYA-104 revealed a yield of 32.38 % and 9.09 %, respectively. For sand sample SXQ-102, this value can be justified because for this process it was taken a previously sieved sample.
- Characterization of enriched sands by AAS, EDS, and XRD confirmed that sand sample SXQ-102 presented a major percentage of iron than SYA-104. Also, the minerals present in the enriched samples were iron and titanium oxides accompanied by silicates composed by Si, Al, Mg, Na, and Ca.

- Reactivity of enriched sands with hydrogen sulfide was carried out in a semi-hermetic system sealed with a septum. The sand sample presented a change in its color, from black to greenish-yellow.
- The chemical comparison between both enriched and reacted sands indicates that sample SYA-104 adsorbed acid on its surface than sample SXQ-102 which is indicated in the pH test. After the analysis in XRD, sample SYA-104 showed the presence of titanium sulfate, which would explain the acidity of this sand.

7.2. Recommendations

- The septum used to cover the round bottom flask does not completely retain the acid gas; in fact, a gas leak was found during the reactivity process. So, it is required to design a more hermetic system for the reactivity of the sands, so that the gas remains inside and react totally with the surface of the sands.
- It is recommended to do a new sampling field trip to the Coastal zone and in Cotopaxi province covering the areas not sampled before, and intensifying it in the areas around the Quilotoa volcano and around the Anconcito county.

BIBLIOGRAPHY

- (1) Organization of the Petroleum Exporting Countries. Ecuador Facts and Figures https://www.opec.org/opec_web/en/about_us/148.htm, accessed in January, 2020.
- (2) Ministry of the Environment. Economics of Greenhouse Gas Limitations. *Ctry. Study Ser.* **1999**, 6, 1–205.
- (3) Banco Central del Ecuador. *Participación Porcentual de los Principales Productos de Exportación (IEM-312b-E_)*, 2019.
- (4) Host, K. Extracción del Petróleo. In: *Petróleo*; 2017; pp 1–11.
- (5) Ricaurte, M.; Fernández, J. M.; Vilorio, A. An Improved Method for Calculating Critical Temperatures and Critical Pressures in Natural Gas Mixtures With up to nC11 Hydrocarbons. *Oil Gas Sci. Technol.* **2019**, 74. <https://doi.org/10.2516/ogst/2019027>.
- (6) Amer, E. Natural Gas Composition. *Explore* **2019**, 1–33.
- (7) Mokhatab, S.; Poe, W. A.; Mak, J. Y. Basic Concepts of Natural Gas Processing. In *Handbook of Natural Gas Transmission and Processing*; Elsevier Inc., 2015; pp 123–135. <https://doi.org/10.1016/B978-0-12-801499-8.00003-1>.
- (8) Danbury, C. Hydrogen Sulfide Safety Data Sheet P-4611. *Praxair* **2016**, 10.
- (9) Labor, D. *Hydrogen Sulfide (H₂S)*; 2005.
- (10) Chou, C. H. S.; World Health Organization; International Programme on Chemical Safety. Hydrogen Sulfide: Human Health Aspects. *World Heal. Organ.* **2003**, No. 9241530537, 53.
- (11) Barrios, J. Generalidades del Endulzamiento del Gas Natural. Advertisement Similar to Advertisement. *ISUU* **2013**, 18–70.
- (12) Camizán, A. Estudio del Tratamiento de Emisiones Gaseosas de Sulfuro de Hidrógeno a Nivel Piloto e Industrial. *UNMSM* **2015**.
- (13) Higgins, M.; Hewins, M.; Noakes, B. SulfaTreat® -410 HP Select Fast-Reacting Mixed-Metal-Oxide /company/32741/Higgins- and-Hewins/, **2019**.
- (14) Miller, C. *Security Sheet SulfaTreat(R) ST-410-HP.pdf*; Houston, 2002.
- (15) Braga, T. G. SulfaTreat; *Schlumberger* 2004.
- (16) Ricks, K. H₂S Treatment of Landfill Gas at the Roosevelt Landfill. *Klicktat PUD* **2019**, No. 03234–7984, 44.

- (17) Di Felice, R.; Pagliai, P. Prediction of the Early Breakthrough of a Diluted H₂S and Dry Gas Mixture When Treated by SulfaTreat Commercial Sorbent. *Biomass and Bioenergy* **2015**, *74*, 244–252. <https://doi.org/10.1016/j.biombioe.2015.01.015>.
- (18) Tacuri, F. J. Mejoramiento del Proceso de Endulzamiento de Un Gas Utilizado Como Combustible, Universidad Central del Ecuador, 2015.
- (19) Díaz, J. C. Caracterización Geológica y Geofísica de la Zona Oeste de la Concesión Minera Mompiche, Ubicada en la Provincia de Esmeraldas, Cantón Muisne, Recinto Mompiche, Escuela Politécnica Nacional, 2013. <https://doi.org/10.1103/PhysRevX.7.041008>.
- (20) Centro Politécnico Vigo. Efecto de los Agentes Geológicos Externos. In: *Procesos Geológicos*; 2019; pp 3–7.
- (21) Collot, J.-Y.; Sallares, V.; Pazmiño, N. *Geología y Geofísica Marina y Terrestre del Ecuador*; Institut de recherche pour le développement, 2009.
- (22) Holt, R.; Holt, W. Shoreline Erosion and Deposition. In: *Earth's Changing Surface*; 2019; pp 39–45.
- (23) Welch, B. K. The Occurrence and Paragenesis of the Ores of Titanium, Durham University, 1958.
- (24) Meneses, E. Valoración Económica de los Servicios Recreativos de la Playa Negra en la Zona del Ostional., Pontificia Universidad Católica del Ecuador, 2017.
- (25) Ahmad, S.; Rhamdhani, M. A.; Pownceby, M. I.; Bruckard, W. J. 10 Sulfidising Roast Treatment for the Removal of Chrome Spinels from Murray Basin Ilmenite Concentrates. *International Journal of Mineral Processing* **2014**, 36–39.
- (26) Toro, J.; Ayala, C.; Chimarro, M.; Caetano, M.; Ricaurte, M. Organic Processes Controlling Grain-Size and Granulometric Parameters of Beach Sands in Coastal Ecuador. In *REDU, Diseño, Arte, Geo-ciencias, Arqueología, Paleontología, Arquitectura, Patrimonio, Ciudad, Teritorio y Geo-parques*; Universidad Yachay Tech, 2019; Vol. 1, pp 1–36.
- (27) Toro, J. *Muestreo-Protocolo de Toma de Muestras de Suelo*; 2018.
- (28) Ramírez, J. Estudio de las Transformaciones de las Fases Cristalinas de las Arcillas en el Proceso de Quema de la Cerámica, Universidad Central del Ecuador, 2019.
- (29) Kobya, M.; Demirbas, E.; Bayramoglu, M. Modelling the Effects of Adsorbent Dose and Particle Size on the Adsorption of Cr(VI) Ions from Aqueous Solutions. *Adsorpt. Sci. Technol.* **2004**, *22* (7), 583–594. <https://doi.org/10.1260/0263617042879465>.
- (30) Koirtzmann, S. R. A History of Atomic Absorption Spectroscopy. *Spectrochim.*

Acta **1980**, 35, 663–670.

- (31) Royal Society of Chemistry. Atomic Absorption Spectrometry. *Anal. Chem.* **1980**, 52 (9), 1079–1080. <https://doi.org/10.1021/ac50059a771>.
- (32) SHIMADZU Corporation. Atomic Absorption Spectrophotometry Cookbook Section 1: Basic Conditions of Analysis of AAS. **2027**, 44–72.
- (33) Villashañay, J.; Vásquez, C. Atomic Absorption Spectrophotometry Guide; *Inst. Nac. Patrim. Cul.* 2017.
- (34) INPC. Digestión de Arenas Y Arcillas. *Inst. Nac. Patrim. Cul.* **2019**, Quito.
- (35) Pérez, A. Equipo Experimental Y Técnicas de Caracterización, Universitat de Barcelona, 2018.
- (36) Girão, A. V.; Caputo, G.; Ferro, M. C. Application of Scanning Electron Microscopy–Energy Dispersive X-Ray Spectroscopy (SEM-EDS). *Compr. Anal. Chem.* **2017**, 75, 153–168. <https://doi.org/10.1016/bs.coac.2016.10.002>.
- (37) Chauhan, A. Powder XRD Technique and Its Applications in Science and Technology. *J. Anal. Bioanal. Tech.* **2014**, 5 (6). <https://doi.org/10.4172/2155-9872.1000212>.
- (38) Carrera, E.; Estrella, A. Diseño y Construcción de un Separador Magnético para Minerales, Universidad del Azuay, 2018.
- (39) Stafeev, A. A. Iron-Ore Enrichment by Magnetic Hydroseparation. *Steel Transl.* **2011**, 41 (10), 823–825. <https://doi.org/10.3103/S0967091211100214>.
- (40) Macherey-Nagel. pH.Fix Test Strips www.mn-net.com, Accessed in February, 2020..
- (41) Rosi, M.; Landi, P.; Polacci, M.; Di Muro, A.; Zandomenighi, D. Role of Conduit Shear on Ascent of the Crystal-Rich Magma Feeding the 800-Year-B.P. Plinian Eruption of Quiltoea Volcano (Ecuador). *Bull. Volcanol.* **2004**, 66 (4), 307–321. <https://doi.org/10.1007/s00445-003-0312-z>.
- (42) Gardner, J. E.; Rutherford, M.; Carey, S.; Sigurdsson, H. Experimental Constraints on Pre-Eruptive Water Contents and Changing Magma Storage prior to Explosive Eruptions of Mount St Helens Volcano. *Bull. Volcanol.* **1995**, 57 (1), 1–17. <https://doi.org/10.1007/BF00298703>.
- (43) Soledispa, B. Características de La Sedimentación Marina Litoral Comprendida Entre La Puntilla de Santa Elena Y Punta Ancón. Provincia de Santa Elena, Ecuador. *Acta Ocean. del PACÍFICO* **2017**, 14 (1), 181–188.
- (44) Federici, P. R.; Rodolfi, G. Rapid Shoreline Retreat along the Esmeraldas Coast,

- Ecuador: Natural and Man-Induced Processes. *J. Coast. Conserv.* **2001**, 7 (2), 163–170. <https://doi.org/10.1007/BF02742478>.
- (45) Yin, L. Dynamic Light Scattering. *Nanotechnol. Res. Methods Foods Bioprod.* **2012**, 145–161. <https://doi.org/10.1002/9781118229347.ch8>.
- (46) Miller, J. N.; Miller, J. C. *Statistics and Chemometrics for Analytical Chemistry*, 6th ed.; Pearson Education Limited: England, 2010.
- (47) Gražulis, S.; Daškevič, A.; Merkys, A.; Chateigner, D.; Lutterotti, L.; Quirós, M.; Serebryanaya, N. R.; Moeck, P.; Downs, R. T.; LeBail, A. Crystallography Open Database (COD): An Open-Access Collection of Crystal Structures and Platform for World-Wide Collaboration. *Nucleic Acids Res.* **2012**, 40, 420–427. <https://doi.org/10.1093/nar/gkr900>.
- (48) Merkys, A. .; Vaitkus, A. .; Butkus, J. .; Okulič-Kazarinas, M. .; Kairys, V.; Gražulis, S. COD::CIF::Parser: An Error-Correcting CIF Parser for the Perl Language. *J. Appl. Crystallogr.* **2016**, 49. <https://doi.org/10.1107/S1600576715022396>.
- (49) Quirós, M. .; Gražulis, S. .; Girdzijauskaitė, S. .; Merkys, A.; Vaitkus, A. Using SMILES Strings for the Description of Chemical Connectivity in the Crystallography Open Database. *J. Cheminformatics, Springer Nat.* **2018**, 10, 10. <https://doi.org/10.1186/s13321-018-0279-6>.
- (50) Gražulis, S.; Merkys, A.; Vaitkus, A.; Okulič-Kazarinas, M. Computing Stoichiometric Molecular Composition from Crystal Structures. *J. Appl. Crystallogr.* **2015**, 48, 85–91. <https://doi.org/10.1107/S1600576714025904>.
- (51) Turkekul, I.; Elmastas, M.; Tüzen, M. Determination of Iron, Copper, Manganese, Zinc, Lead, and Cadmium in Mushroom Samples from Tokat, Turkey. *Food Chem.* **2004**, 84 (3), 389–392. [https://doi.org/10.1016/S0308-8146\(03\)00245-0](https://doi.org/10.1016/S0308-8146(03)00245-0).
- (52) Piedrahita, O. Introducción pH Del Suelo. *Magnesio Heliconia S.A.* **2009**, 14 (cuadro 1).
- (53) Peterman, M.; Benhabib, M.; Kleinman, S. Portable, Rapid Analysis of MEA-Triazine via Raman Spectroscopy <https://slideplayer.com/slide/15321919/>.
- (54) Algonquin, E. *UOP MOLSIVTM Molecular Sieves for Gas Processing*; 2016.
- (55) Peskov, M. Zeolites <http://asdn.net/asdn/chemistry/zeolites.php>.

ANNEXES

Annex A

Sweetening of natural gas

The sweetening of natural gas consists of the purification process in which the amounts of acid gases, such as hydrogen sulfide (H₂S) and carbon dioxide (CO₂), are controlled. It is important to remove the H₂S because it is harmful to human health; also, it causes corrosion to the facilities. Currently, there exist several methods for trapping H₂S from natural gas. The selection of the best option to sweeten the natural gas will depend on the applicability of the method, the economy involved in the process, and the effectiveness. The amount of acid that will be removed will depend on the sweetening method chosen¹¹. Among the techniques used to capture hydrogen sulfide are¹¹:

Acid gases absorption

Absorption is a process in which the gas (or vapor) is retained by another substance that can be liquid or solid. This method is applied in gases with low partial pressure. In addition, this process is used to remove some gases from the gas flow; such as acid gases, hydrocarbon vapor, water vapor, etc. Among acid gases, H₂S is the first gas to be removed, then, it is followed by CO₂. Some of the conditions for this method are the control of known/established temperature, pressure, volume and composition of the gas, the selectivity of the gases to be removed, among others. Acid gas absorption can occur in a chemical, physical or mixed way.

Chemical absorption

Also known as absorption with amines, this process involves the chemical reaction of the acid component with an active component in the solution. Usually, the most used solvent is through amines, which are organic compounds derived from ammonia, with the ability to form hydrogen bonds.

In the sweetening of natural gas, the amines commonly used are: monoethanolamine (MEA), diglicolamine (DGA), diethanolamine (DEA), triethanol amine (TEA), methyldiethanolamine (MDEA), and di-isopropanol amine (DIPA). MEA, DEA, and TEA are low volatility compounds with hygroscopic capacity. DGA is a very stable amine that shows a high degradation degree in the presence of sulfur compounds. MDEA is slightly

toxic for skin amine that slowly reacts with CO₂, it removes better H₂S. DIPA is considered non-corrosive molecule that presents low requirements for the regeneration solution.

Chemical solvents have a good efficiency to eliminate acid gases; however, its solutions use to present corrosive nature, the energy demand is too high, and the charge of the acid gas in solution is limited.

Physical absorption

The physical absorption of gases depends on the solubility, temperature, and partial pressure of the gas. This technique is applied in a high pressure process which results in greater efficiency. Solvents used in this method are not corrosive and dehydrate with a greater selectivity to H₂S. Also, physical solvents can remove heavy hydrocarbons, like hydrogen cyanide (HCN), and sulfur organic compounds.

Physical solvents do not chemically react with solute, so they consume less energy to absorb acid gases. However, since the interaction between solute and solvent is weak, the loss of gases as products is possible.

Physical-chemical absorption

This method uses both chemical and physical solvents, so its procedure will show properties characteristic of both. This kind of solvents can remove all the acid gases, such as: H₂S, CO₂, COS, CS₂, RSH, and heavy hydrocarbons.

Despite the benefits offered by the acid gas absorption method, the process for natural gas sweetening presents some drawbacks; one of them is foaming which affects the efficiency of the process. Main causes for foaming are solids in suspension, organic solids, condensed hydrocarbon, soapy fats, and other impurities. However, foaming can be controlled by adjusting the values for pressure, foam height, and contact angle to increase its efficiency¹¹.

Direct conversion

Direct conversion method consists of the transformation of the hydrogen sulfide to sulfur by using tail gases in a natural way. The resulting sulfur is used to obtain sulfuric acid and oil compounds. The process involves redox scales starting with the absorption of H₂S in an alkaline solution; then, the oxidation of H₂S caused by sodium meta-vanadate (NaVO₃) to

obtain sulfur (S). After that, the vanadate is oxidized by anthraquinon disulfonic acid (ADA), which finally is reduced by the action of air¹¹.

Chemical Captors

Chemical captors are compounds that react with hydrogen sulfide to form products that can be discarded more easily. They can be solid or liquid.

Solid

Solid chemical captors known are iron oxides, zinc oxides, among others. In this process, the solid captor decomposes the hydrogen sulfide (H₂S) to produce elemental sulfur (S) and iron sulfide (FeS) eliminating a big amount of hydrogen sulfide.

Liquids

Liquid chemical captors can be nitrates, amine-aldehyde condensates like triazine, etc. Indeed, triazine can react with hydrogen sulfide to form one molecule of dithiazine and two amines (see Figure 31). This captor can be injected directly in the flow lines or in the contact tower.

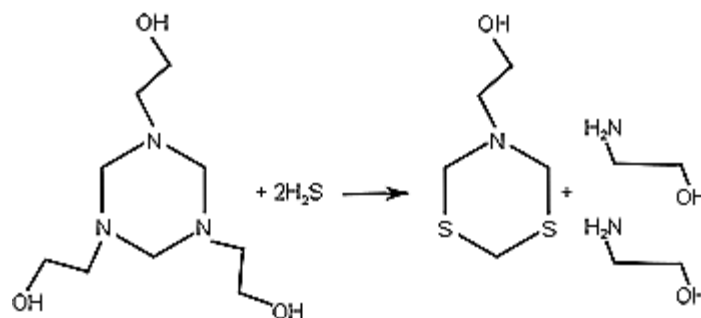


Figure 31: Triazine captor and hydrogen sulfide reaction⁵³.

Semipermeable membranes

Semipermeable membranes are used to remove impurities from natural gas based on the affinity, and diffusivity differences. The separation of gases is not complete, that is to say, that there will be a loss of compounds of natural gas.

Extractive distillation

This process consists of the alteration of the relative volatility of a compound caused by a separation agent which is no volatile and presents an elevated boiling point with the purpose of separate the components. The extractives distillation requires a solvent with the following characteristics:

- High selectivity to alter the liquid-vapor equilibrium
- High capacity to dissolve the components of the mixture
- Low volatility to avoid evaporation
- Easy to separate from the mixture
- Economic, not toxic, and chemically stable.

Solid beds

Solid beds are products commonly used in gas industries. The acid gases removal is realized by an adsorption process which, depending on the material surface to use, it can be chemical or physical¹². This technique uses, as solid beds, molecular sieves, iron sponge, zinc oxide, or SulfaTreat®. For beds made of solid beds, iron, and zinc oxides, the reaction is chemical and irreversible; while, for molecular sieves, the reaction is physical and reversible¹².

Molecular sieves

Molecular sieves are silicate sieves that present a three-dimensional microporous crystalline structure similar to the Zeolite structure (see Figure 32) which allows the removal of acid impurities when natural gas flows through it. This material is able to selectively adsorb the acid gas by its size and polarity. Depending on the application, the shape, size, and type, molecular sieve varies. Among the most common uses of this material are natural gas CO₂ removal, natural gas desulfuration, natural gas dehydration, and others⁵⁴.

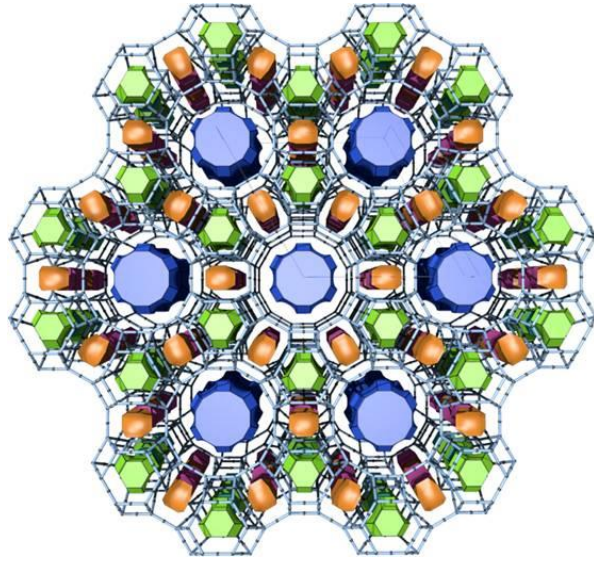


Figure 32: Tiling representation of the structure of the zeolite L (LTL). Blue tiles are channels in the structure running along the direction of the crystallographic c axis⁵⁵.

Iron sponge

The iron sponge is a solid bed consisted of wood chips impregnated by ferric oxide. This is a selective method for sulfur components or oxidant agents. Chips serve as a spongy agent to allow the natural gas flow and better contact of the iron oxide with the acid gas.

This method is not recommended to eliminate elevated amounts of H_2S , it only can be applied to gases with a concentration lower than 320 ppm.

Zinc oxides

The use of zinc oxides is considered a dry bed process that works at temperatures between 300-700 °C. At that temperature, the sulfidation of zinc oxide (ZnO) and the formation of sulfur (S) happen in the presence of H_2S . The oxidation of sulfur (from S^{-2} to S) is due to the presence of water. Nowadays, this process is less used because zinc oxides present loss of surface area.

SULFATREAT®-410 HP

SulfaTreat® is a sandy solid material coated by iron oxides very selective to remove hydrogen sulfide. It works at lower temperatures than zinc oxides, between 18-25 °C, and resists up to 100 ppm of hydrogen sulfide. This material is environmentally friendly and its maintenance must be performed every 330 days¹¹.

Annex B

Table 13: Water presence and water loss percentages of the natural sand samples according to the time of drying.

Sample	% Water in sample	% Water loss	Time (h)
SXQ-101	99,53	0,47	4
SXQ-102	99,70	0,30	4
SYA-103	96,55	3,45	5
SYA-104	98,06	1,94	5
SYO-105	82,59	17,41	9
SYM-106	86,72	13,28	5
SEV-201	73,17	26,83	13
SET-202	83,06	16,94	5
SET-203	81,80	18,20	5
SMP-204	85,42	14,58	5
SEM-205	81,63	18,37	5
SEM-206	81,48	18,52	6
SEG-207	81,90	18,10	5

Annex C

Table 14: Total concentration of iron in the sand sample determined by Atomic Absorption Spectrophotometry.

	Sample ID	Conc. (ppm)±7	Abs.	%Fe±0.2	*Conc.(mg/mL)
STD	40		0.066		
STD	120		0.173		
STD	200		0.254		
UNK1	SXQ-101	177	0.231	5.1	17.68
UNK2	SXQ-102	155	0.206	17.9	62.18
UNK3	SYA-103	103	0.144	2.8	10.27
UNK5	SYA-104	121	0.165	13.2	48.23
UNK6	SYO-105	30	0.058	0.8	2.95
UNK7	SYM-106	114	0.157	6.7	22.75
UNK8	SEV-201	79	0.116	4.6	15.77
UNK9	SET-202	71	0.107	2.0	7.12
UNK10	SET-203	57	0.090	1.7	5.67
UNK11	SMP-204	104	0.146	2.9	10.44
UNK12	SEM-205	95	0.135	2.5	9.50
UNK13	SEM-206	73	0.109	2.0	7.29
UNK14	SEG-207	95	0.135	2.5	9.50

Annex D

XRD results for all natural sands. Inset include the percentage of mineral phases present in the samples.

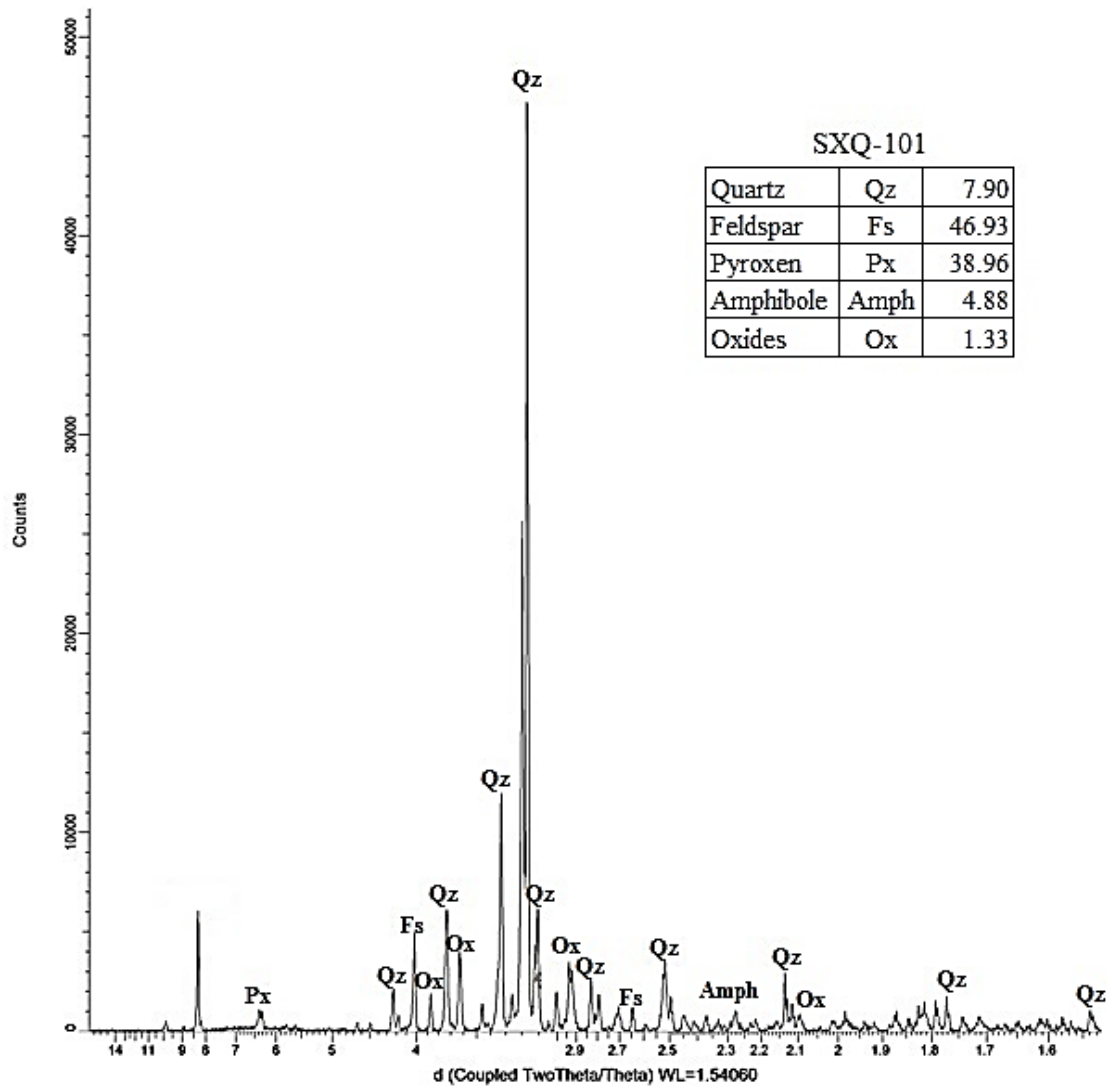


Figure 33 : X-ray diffraction pattern for natural sand sample SXQ-101. The inset includes the percentage of mineral phases in the sample.

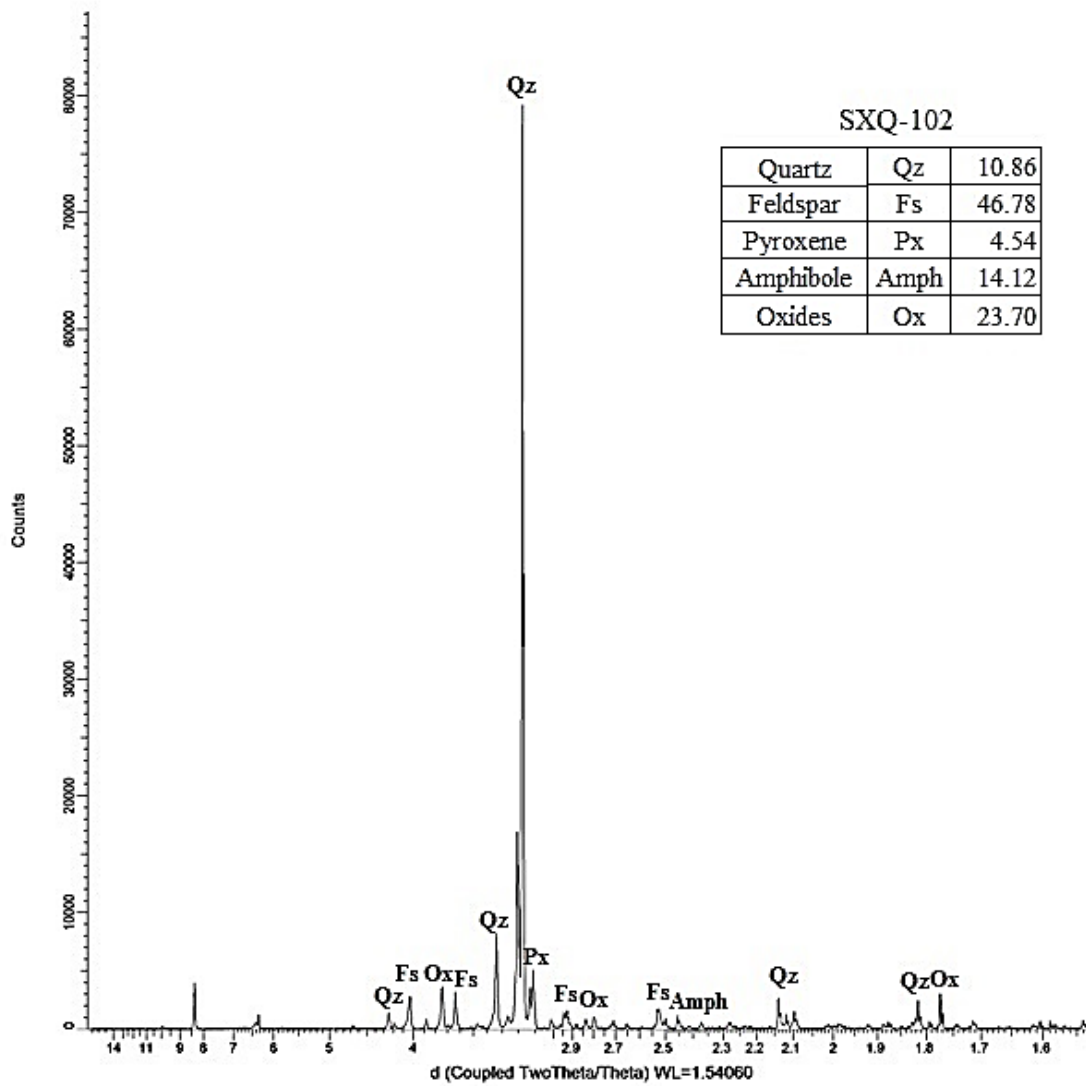


Figure 34: X-ray diffraction pattern for natural sand sample SXQ-102. The inset includes the percentage of mineral phases in the sample.

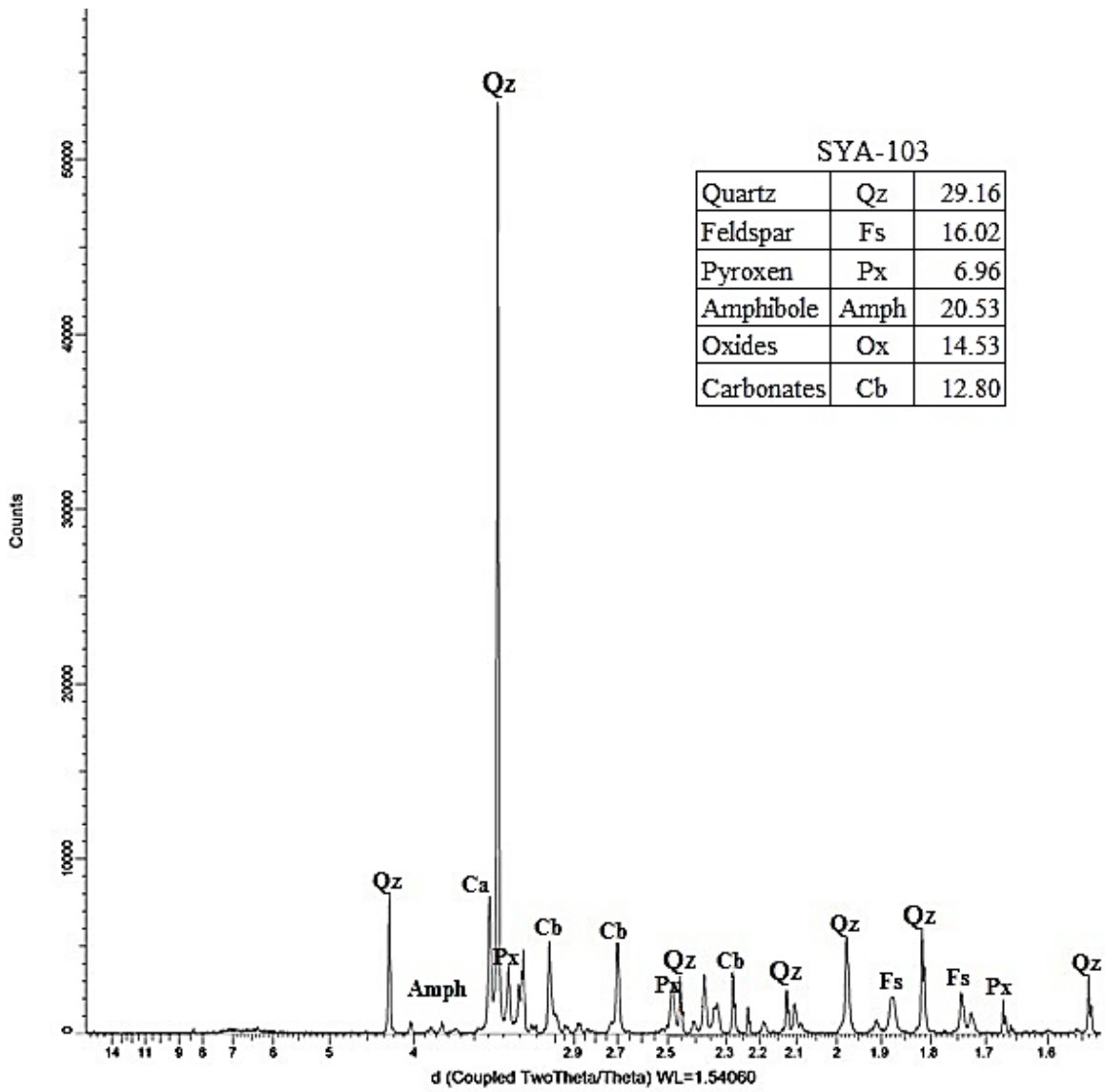


Figure 35: X-ray diffraction pattern for natural sand sample SYA-103. The inset includes the percentage of mineral phases in the sample.

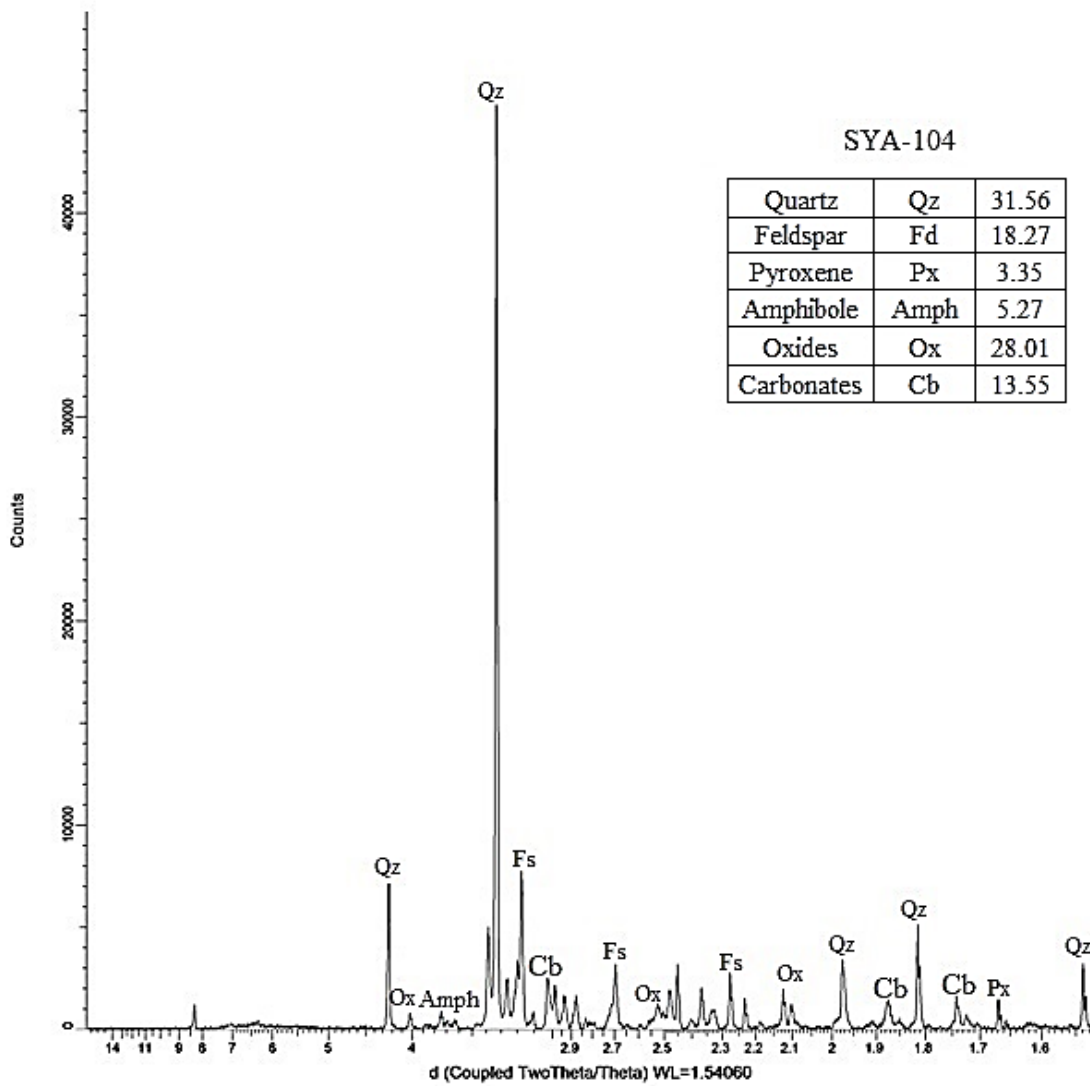


Figure 36: X-ray diffraction pattern for natural sand sample SYA-104. The inset includes the percentage of mineral phases in the sample.

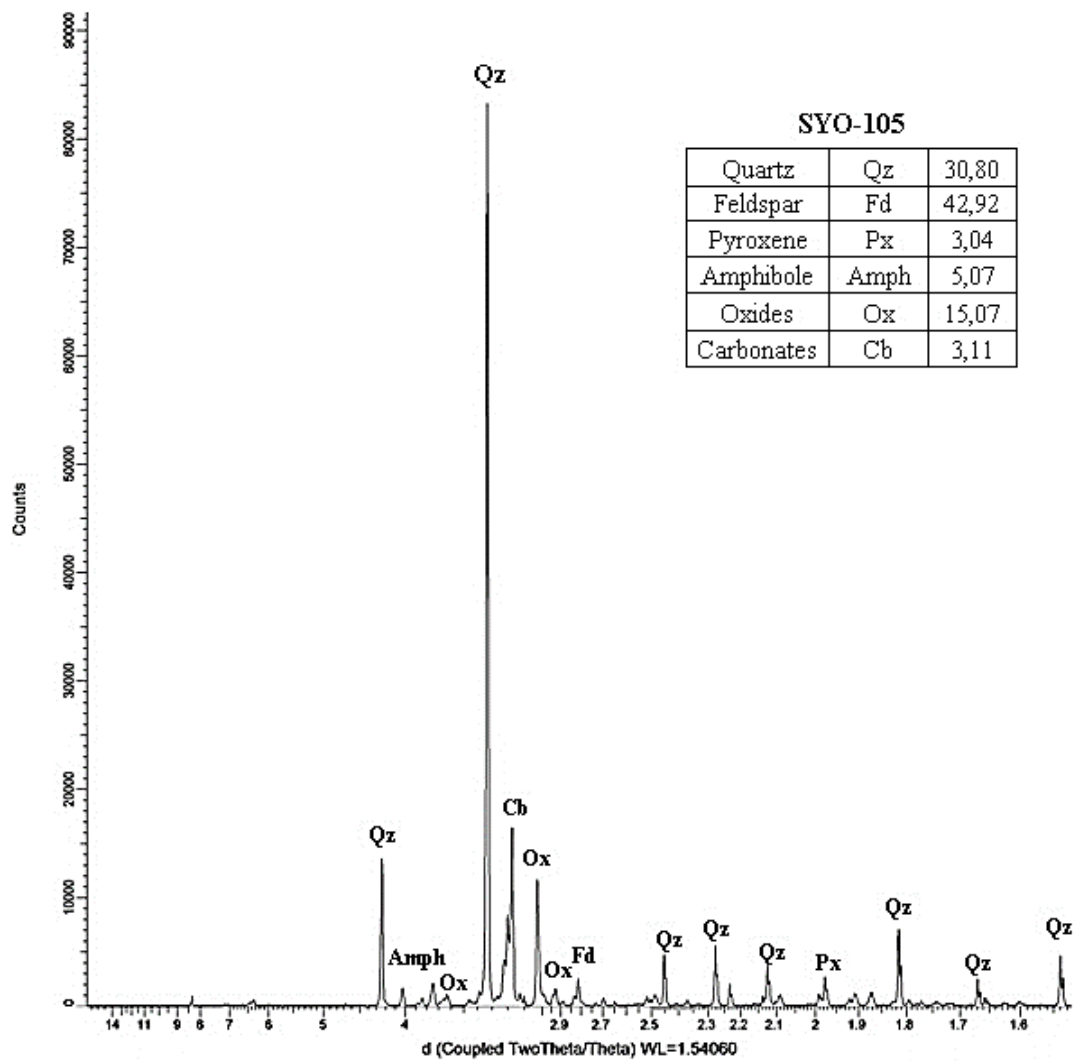


Figure 37: X-ray diffraction pattern for natural sand sample SYO-105. The inset includes the percentage of mineral phases in the sample.

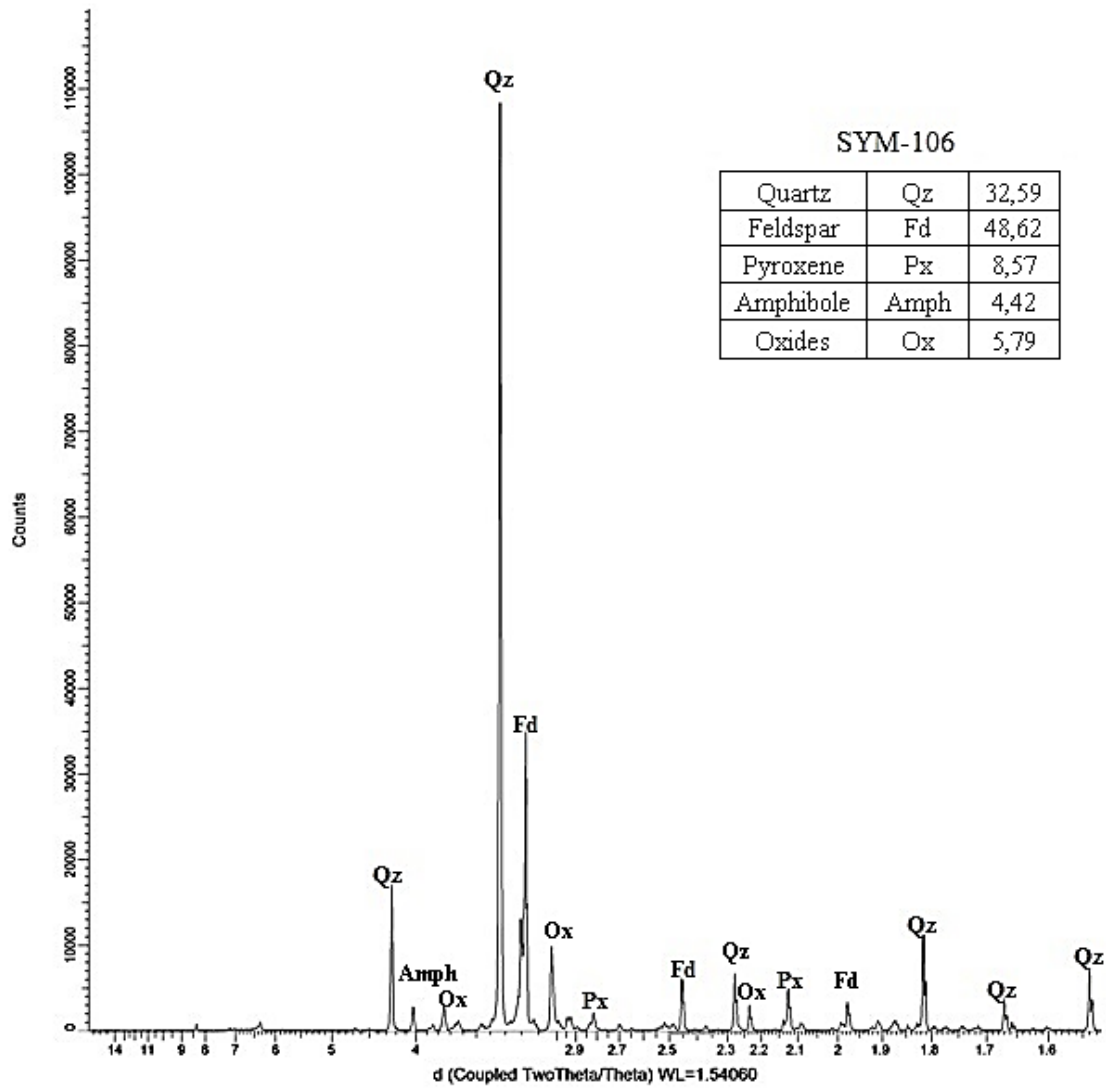


Figure 38: X-ray diffraction pattern for natural sand sample SYM-106. The inset includes the percentage of mineral phases in the sample.

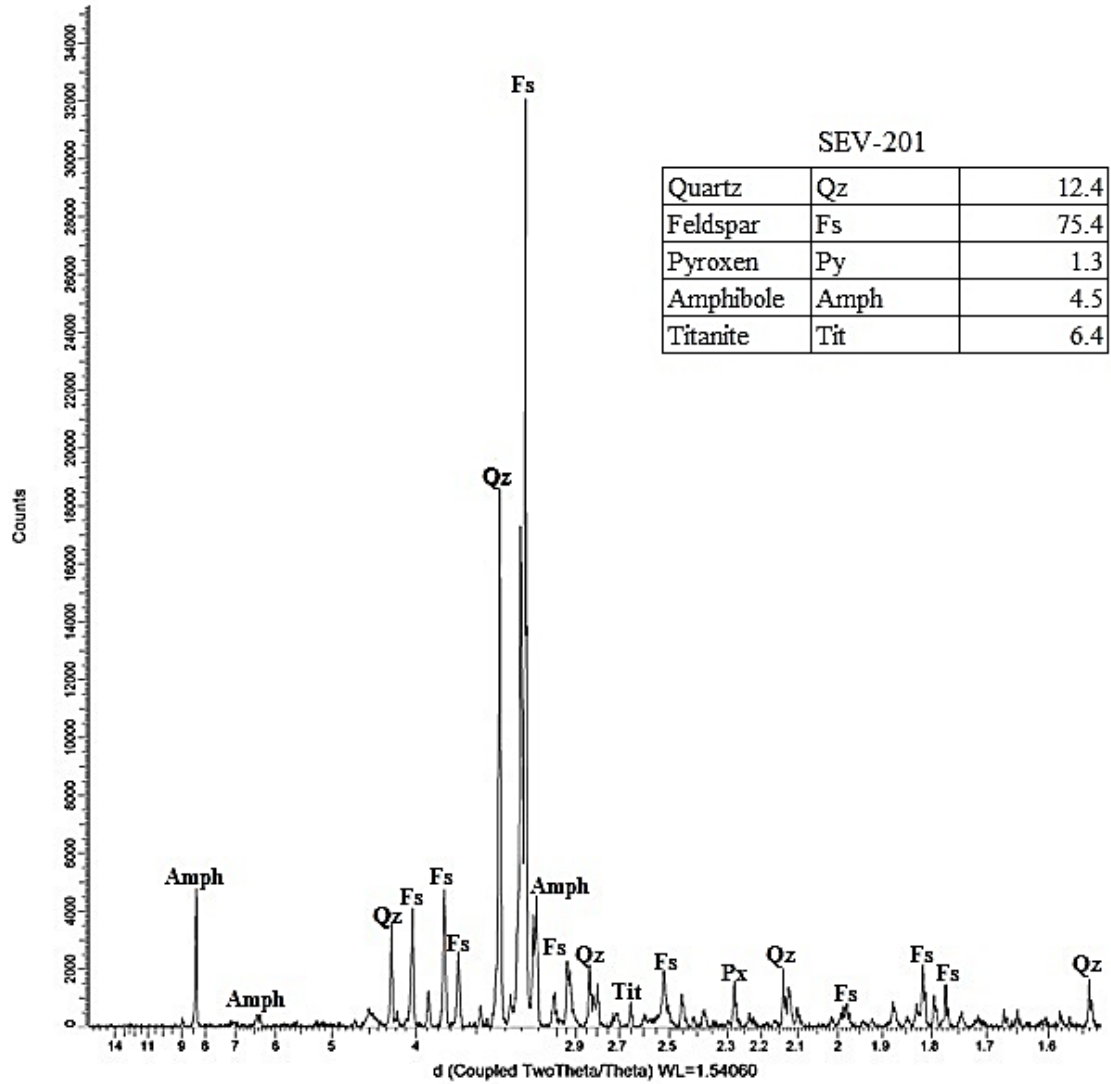


Figure 39: X-ray diffraction pattern for natural sand sample SEV-201. The inset includes the percentage of mineral phases in the sample.

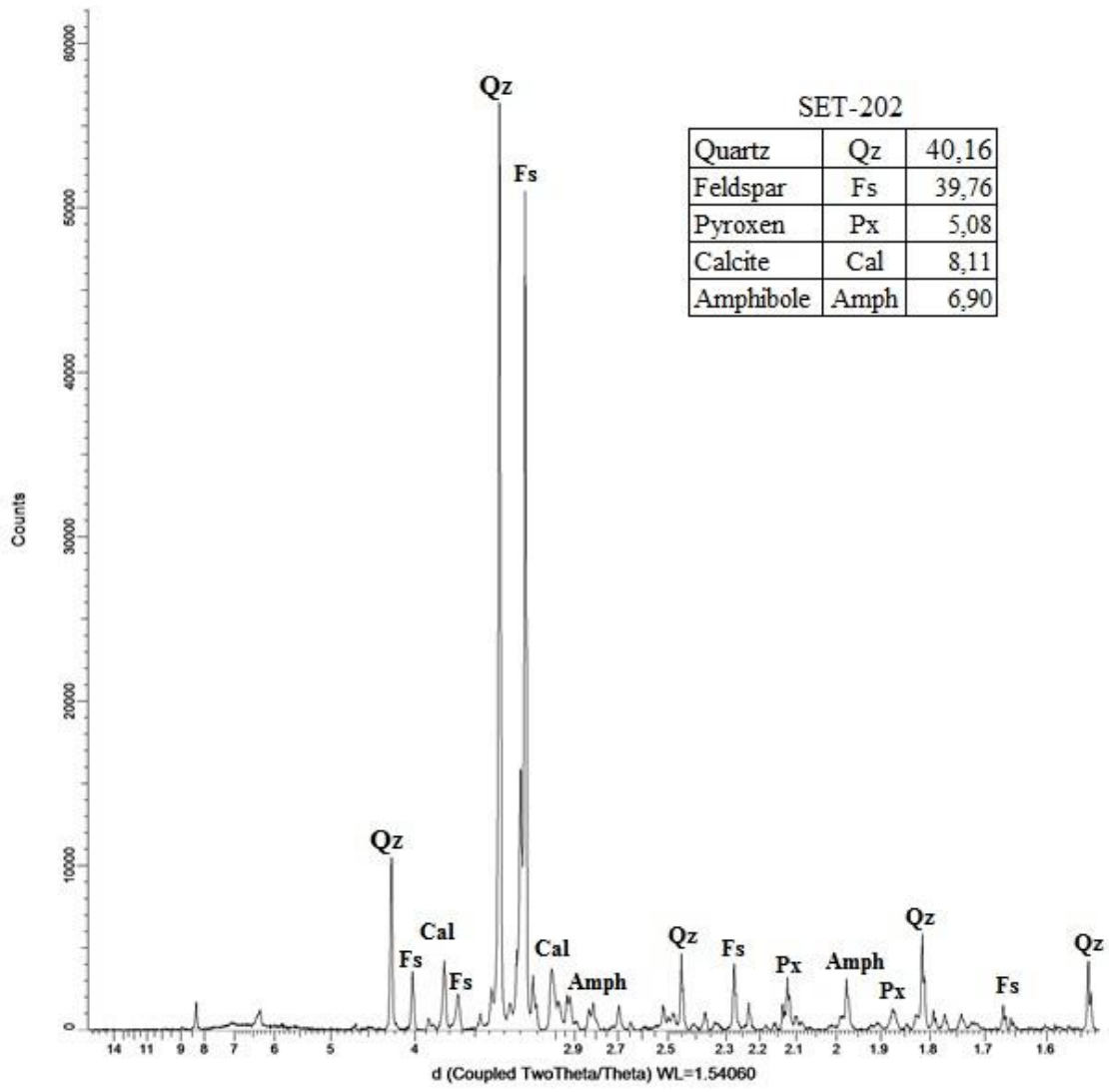


Figure 40: X-ray diffraction pattern for natural sand sample SET-202. The inset includes the percentage of mineral phases in the sample.

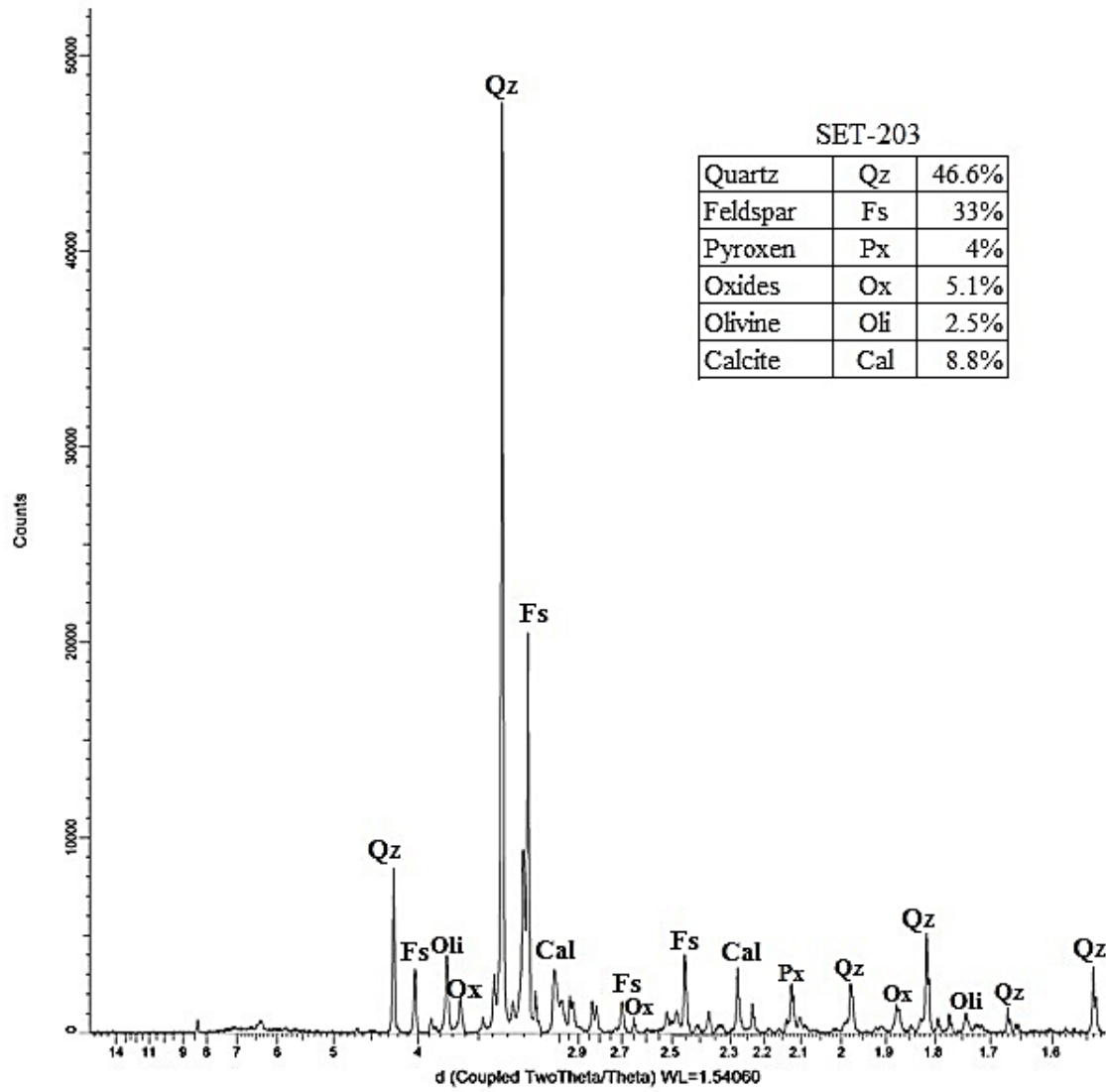


Figure 41: X-ray diffraction pattern for natural sand sample SET-203. The inset includes the percentage of mineral phases in the sample.

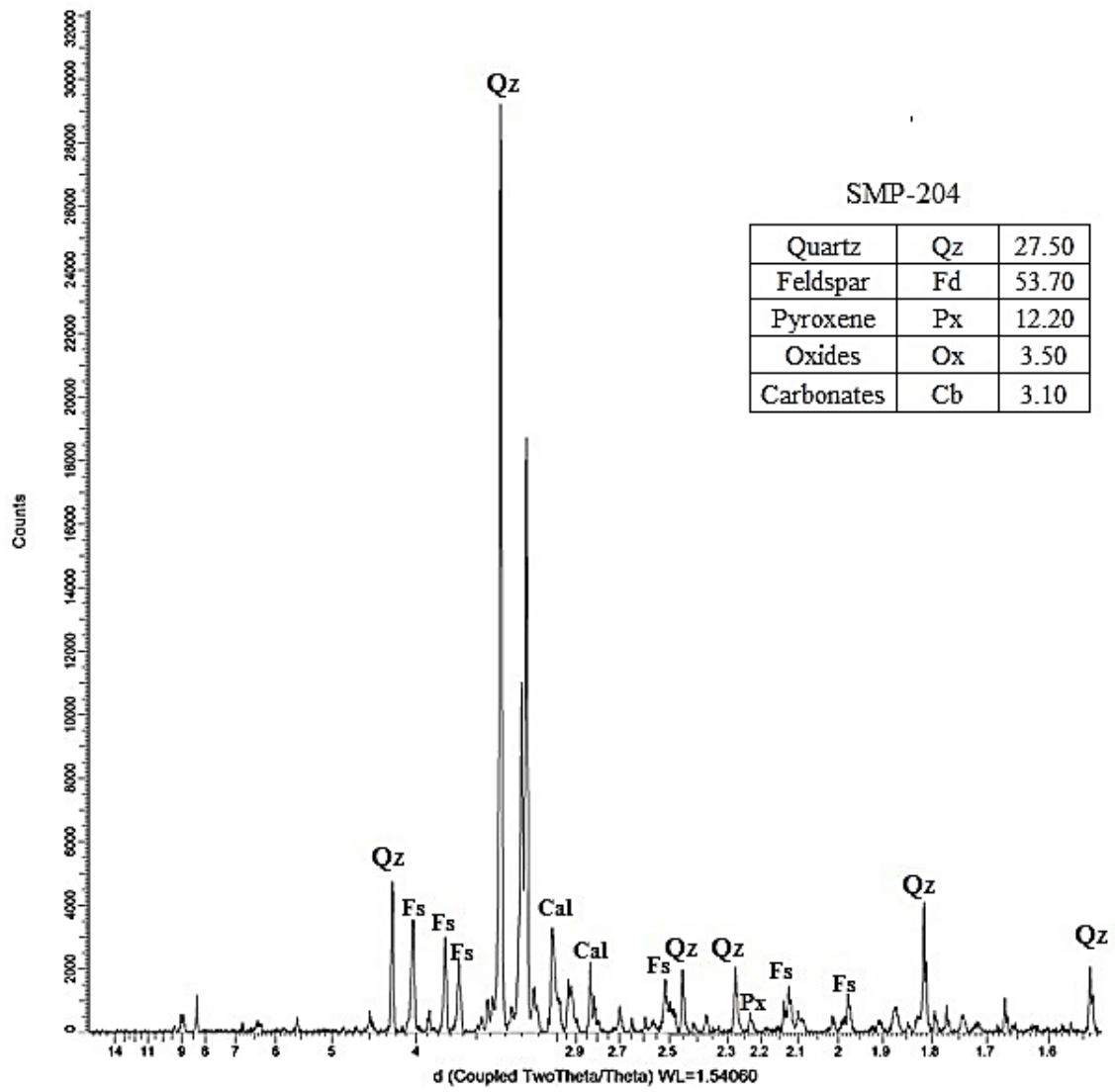


Figure 42: X-ray diffraction pattern for natural sand sample SMP-204. The inset includes the percentage of mineral phases in the sample.

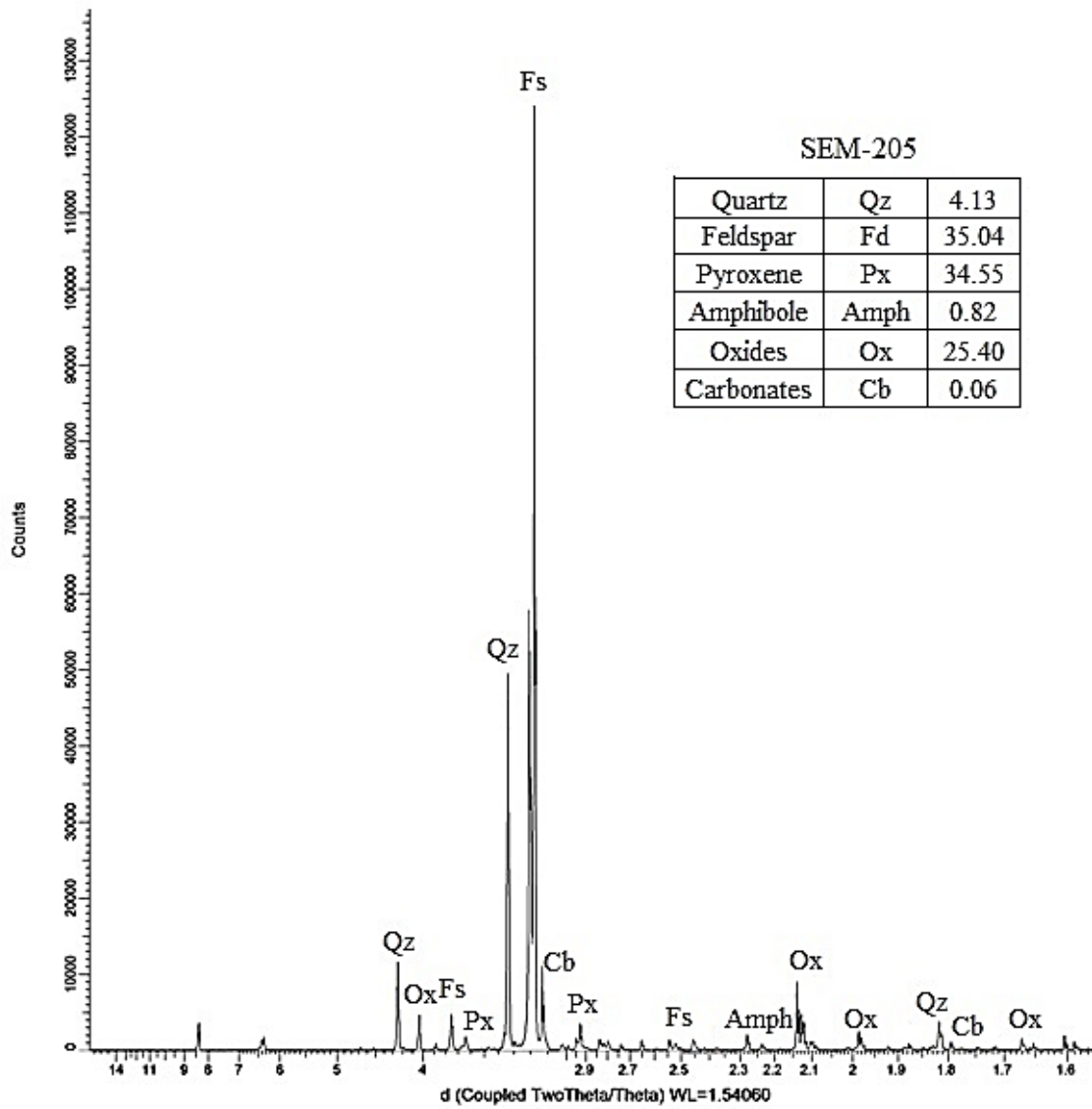


Figure 43: X-ray diffraction pattern for natural sand sample SEM-205. The inset includes the percentage of mineral phases in the sample.

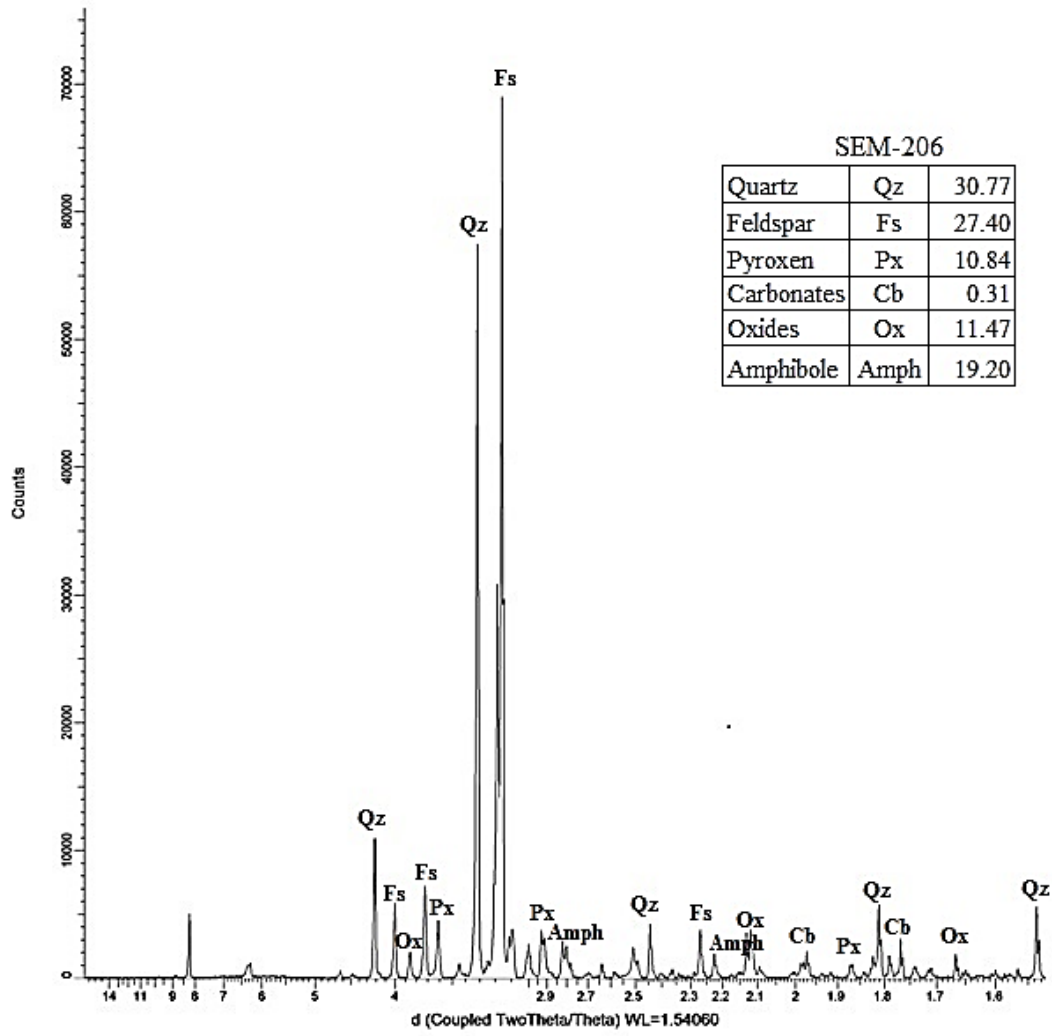


Figure 44: X-ray diffraction pattern for natural sand sample SEM-206. The inset includes the percentage of mineral phases in the sample.

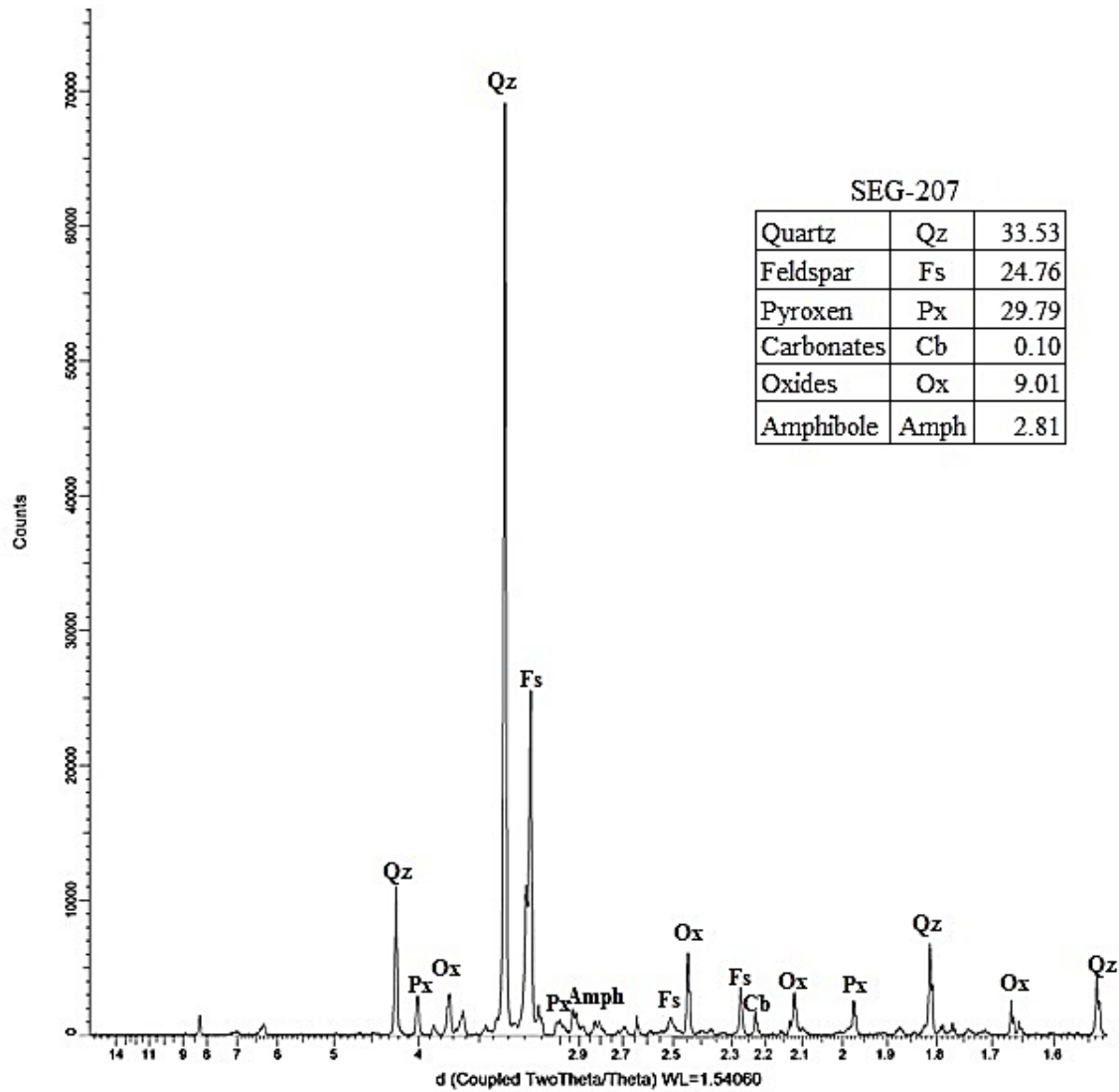


Figure 45: X-ray diffraction pattern for natural sand sample SEG-207. The inset includes the percentage of mineral phases in the sample.

